ELSEVIER

Contents lists available at ScienceDirect

### Electrochimica Acta

journal homepage: www.elsevier.com/locate/electacta



Review Article

# Nanostructured Garnet-type Li<sub>7</sub>La<sub>3</sub>Zr<sub>2</sub>O<sub>12</sub>: Synthesis, Properties, and Opportunities as Electrolytes for Li-ion Batteries



Candace K. Chan\*, Ting Yang, J. Mark Weller

Materials Science and Engineering, School for Engineering of Matter, Transport and Energy, Arizona State University, 501 E Tyler Mall, ECG 301, Tempe, AZ 85287-6106, USA

#### ARTICLE INFO

Article history: Received 30 June 2017 Received in revised form 21 August 2017 Accepted 22 August 2017 Available online 25 August 2017

Keywords:
Garnet-type solid electrolyte
Nanowires
Electrospinning
NMR
Composite polymer electrolyte

#### ABSTRACT

The garnet-type Li $^+$  ion conductor Li $_7$ La $_3$ Zr $_2$ O $_{12}$  (LLZO) is a promising candidate as a solid electrolyte for all-solid-state Li-ion batteries. Significant progress towards understanding the structure and properties of LLZO, conventionally synthesized using solid state reaction methods, has already been made in the last decade. The aim of this review is to summarize recent efforts on the synthesis of nanostructured LLZO, with a focus on electrospinning, cellulose templating, and low-temperature (< 900 °C) sol-gel based methods, as well as to highlight the unique properties of nano-sized LLZO. Further research is still needed to fully understand the potential benefits of using nanostructured LLZO in pellet-type, ceramic electrolytes, but a natural opportunity for nanostructured LLZO is in the role of ceramic filler within solid composite polymer electrolytes (CPEs). The current status of CPEs embedded with LLZO ceramic fillers is summarized, including the elucidation of Li $^+$  transport pathways using nuclear magnetic resonance (NMR) spectroscopy.

© 2017 Elsevier Ltd. All rights reserved.

#### 1. Introduction

Because Li-ion batteries contain the highest energy density of commercially available rechargeable energy storage systems, they are attractive for supplying power in portable and vehicular applications. However, Li-ion batteries can fail, catch fire, and/or explode due to abuse from high temperature exposure [1,2], overcharging [3,4], or short-circuiting from lithium dendrite formation [5,6]. One important component of this problem is the flammability and low flashpoints (< 30°C) of the organic carbonate-based solvents comprising the electrolyte [7,8]. This issue has motivated research on the development of Li<sup>+</sup> conducting electrolytes based on polymers, ionic liquids, glasses, or crystalline ceramics to replace the liquid electrolyte and improve the safety characteristics of Li-ion batteries through the implementation of all-solid-state devices [9–12]. Additionally, solid electrolytes have the potential to increase the safety characteristics of Li metal batteries [13], mitigate the problem of polysulfide dissolution from the cathode in Li/sulfur batteries [14], and circumvent the organic electrolyte oxidation problem in Li/oxygen (or Li/air) batteries [15].

Since inorganic materials display superior mechanical properties and thermal stability compared to polymers [10], a great deal

of research has been devoted to the study of ceramic solid electrolytes. To be a suitable solid electrolyte, the ceramic must: 1) display high ionic conductivities, 2) display chemical stability to Liion battery cathodes and anodes, 3) be cost-effective to synthesize, and 4) be easily integrated with the cathode and anode [8]. The first criterion has been a major challenge, as the ionic conductivity of the commonly used electrolyte (1 M LiPF<sub>6</sub> in ethylene carbonate/ diethylene carbonate solvent) is 10<sup>-2</sup> S cm<sup>-1</sup> [16], while the conductivities of solid electrolytes are lower, in the range of 10<sup>-7</sup>- $10^{-3}$  S cm<sup>-1</sup> [9.12]. However, if a dense thin film (e.g.,  $< 100 \mu m$ ) of the solid electrolyte can be prepared, materials with ionic conductivities between  $10^{-4}$ – $10^{-3}$  S cm<sup>-1</sup> can be used in practical applications [14,17]. Many solid electrolytes have also failed the second criterion, a well-known example being the perovskite lithium lanthanum titanate, (Li,La)TiO<sub>3</sub>, which exhibits a high bulk conductivity of  ${\sim}10^{\text{--}3}~\text{S cm}^{\text{--}1}$  [18] but becomes reduced by lithium metal [19,20].

In 2003, Thangadurai *et al.* reported that garnet-type Li<sup>+</sup> conductors with a cubic structure based on Li<sub>5</sub>La<sub>3</sub>M<sub>2</sub>O<sub>12</sub> (M = Nb, Ta) were stable against reaction with molten lithium, but only displayed a bulk ionic conductivity of  $\sim 10^{-6}$  S cm<sup>-1</sup> at room temperature [21]. The 2007 discovery [22] of the cubic garnet Li<sub>7</sub>La<sub>3</sub>Zr<sub>2</sub>O<sub>12</sub> (LLZO) with relatively high ionic conductivity of  $\sim 10^{-4}$  S cm<sup>-1</sup>, non-reactivity with lithium, and wide voltage stability window (> 5 V vs. Li/Li<sup>+</sup>) generated a great deal of further interest

<sup>\*</sup> Corresponding author. E-mail address: candace.chan@asu.edu (C.K. Chan).

in garnets. Since then, there have been many studies, as summarized in several recent reviews [23–25] exploring the properties of LLZO and its doped derivatives. As a result, LLZO has emerged as one of the most promising solid electrolyte materials for all-solid-state Li-ion batteries.

LLZO is conventionally synthesized using a solid state reaction (e.g., from LiOH or Li<sub>2</sub>CO<sub>3</sub>, La<sub>2</sub>O<sub>3</sub>, and ZrO<sub>2</sub>) requiring high temperatures (>1180°C) and long calcination times (e.g. 36 h) [22]. LLZO adopts two polymorphs with Li<sup>+</sup> ionic conductivities that differ by 2 - 3 orders of magnitude. LLZO with a tetragonal structure (t-LLZO, space group I4<sub>1</sub>/acd), which is the thermodynamically stable phase at room temperature [26], typically exhibits a total ionic conductivity of  $10^{-7} - 10^{-6}$  S cm<sup>-1</sup> [27,28]. The higher ionic conductivity on the order of 10<sup>-4</sup> S cm<sup>-1</sup> is correlated to LLZO with a cubic structure (c-LLZO, space group *Ia-3d*), which in earlier studies was formed inadvertently by doping of Al3+ into the Li+ sites through contamination from the alumina crucibles used during the solid state synthesis [29]. Since then, many syntheses include intentional incorporation of Al3+ as an extrinsic dopant to stabilize the c-LLZO phase at room temperature. Aluminum doping, however, comes with its own issues, including a greater activation energy for Li<sup>+</sup> conduction, likely due to the electrostatic repulsion of the Al<sup>+3</sup> ions in Li<sup>+</sup> sites, which can limit the lithium ion mobility [30]. The substitution of Zr<sup>+4</sup> with Ta<sup>+5</sup> [31] is another popular approach for stabilizing the cubic structure, while using  $Ga^{3+}$  dopants can lead to ionic conductivities  $\sim 10^{-3}$  S cm<sup>-1</sup> [32,33]. In the absence of extrinsic dopants, the t-LLZO to c-LLZO phase transition has been reported to occur between 600 - 650 °C

In addition to exploring the defect chemistry and effect of dopants on the properties of LLZO, there have been substantial efforts focusing on the development of low-temperature synthesis methods for LLZO. Part of the motivation for doing so is to avoid the high calcination temperatures required in solid state synthesis, which can also lead to Li<sup>+</sup> loss through volatilization. Since the lithium content in LLZO has been shown to also play a role in the preferred phase that is adopted [26,35,36], better control of the LLZO composition can be important for obtaining materials with the desired ionic conductivity. Low-temperature synthesis methods, such as sol-gel approaches, can also enable the preparation of nanostructured materials, which may display additional advantageous properties, such as improved sintering and densification behavior.

One observation that has appeared in numerous low-temperature syntheses is that the cubic phase can be stabilized at room temperature in nanostructured forms of LLZO. This will be discussed in more detail in the following sections. The mechanism for the phase stability of c-LLZO at room temperature in nanostructured LLZO is still not completely understood. Other metal oxides with multiple polymorphs (e.g., titania, zirconia) also display similar size dependent phase stabilization due to differences in surface energy and crossovers in polymorphic stability as the surface area of the materials increases [37–40]. It is plausible that a similar phenomenon could account for cubic stabilization of LLZO below a critical size parameter. However, the properties of nanostructured LLZO have still not been fully investigated, and other factors such as surface reactions with H<sub>2</sub>O and CO<sub>2</sub> from the ambient atmosphere could also be playing a role on the phase stability of LLZO [30,34,35,41,42]. To better understand sizedependent properties, well-controlled synthetic routes are needed. The development of nanostructured LLZO with shapecontrolled morphologies, however, is still far from mature, with electrospinning as one of the most promising methods that has been established so far for preparing LLZO with a one-dimensional nanowire or nanofiber morphology [43,44].

Although a decade has passed since LLZO was first reported, the application of LLZO as a ceramic electrolyte in all-solid-state batteries is still met with several practical challenges [17]. For example, LLZO does not form good contacts or interfaces with electrodes [45–47], although this can be addressed through careful engineering of the interfaces to avoid large contact resistances [48–52]. Further, co-sintering with cathode layers has been found to result in inter-diffusion of metal cations at the LLZO/cathode interface, which leads to poor cyclability [53–55]. Intriguingly, lithium metal dendrites have also been observed growing within voids or along grain boundaries of LLZO, despite pellet densities > 97% [48,56–58].

As a result, it is not surprising that since the properties of conventional bulk LLZO are still under investigation, understanding how the properties of LLZO differ when prepared as a nanostructured material compared to the bulk form is still limited. Indeed, the grain size dependence of LLZO on its properties is still not fully established, even at the micron-scale. Cheng et al. conducted comparison studies on large grained (100 - 200 µm) and smaller grained (20 - 40 µm) LLZO and found that small grained LLZO may be more air-stable and resistant to reaction with ambient CO<sub>2</sub> and water vapor [59], while also displaying lower interfacial resistance, higher densification rates, and better cycling behavior than large grained LLZO [60]. However, similar studies extrapolated to nanoscaled grain sizes still need to be performed in a systematic way. Pellets prepared from c-LLZO derived from solid-state reaction [36] compared to one prepared from sol-gel derived LLZO [61] showed that the two pellets, both with similar Li and Al contents and prepared using hot-pressing, displayed similar total ionic conductivities at room temperature. The pellet prepared from sol-gel derived LLZO (average grain size of 260 nm) had higher total conductivity at higher temperatures compared to the pellet made from the solid state reaction derived LLZO (average grain size of 3.3 microns); however, the activation energy for the solgel LLZO was 0.41 eV, which is higher than the one observed in the solid-state reaction LLZO of 0.26 eV, the origin of which is still not understood. Nonetheless, the properties of nanostructured ceramics, such as densification at milder sintering conditions [62,63], decreased impurity segregation to grain boundaries [64], and superplasticity [65] may lead to improved properties in pellets derived from nanostructured LLZO.

While further research is still needed to fully understand the potential benefits of nanostructured LLZO in pellet-type, ceramic electrolytes, a natural opportunity for nanostructured LLZO is in the role of ceramic filler in solid composite polymer electrolytes (CPEs). The application of nano-sized particles as ceramic fillers has already been demonstrated to be effective for enhancing the mechanical stability and ionic conductivity of polymer-based solid electrolytes, but these fillers have mostly comprised of spherical particles of inert or "passive" components without intrinsic Li\* conductivity. Several recent studies using LLZO-embedded into polymer films have revealed different degrees of effectiveness, indicating that more careful design of the CPEs, including the optimization of the LLZO fillers and more detailed mechanistic study of the Li\* transport pathways, may be needed for the development of CPEs with high ionic conductivity.

The aim of this review is to summarize recent efforts on the synthesis of nanostructured LLZO, with a focus on the electrospinning and cellulose templating methods investigated in our group. Other low-temperature (< 900 °C) sol-gel based methods will be reviewed, and recent progress on the utilization of LLZO as a ceramic filler in composite polymer electrolytes will be summarized. Finally, future outlooks and opportunities will be provided.

#### 2. Synthesis Methods for Nanostructured LLZO

#### 2.1. Nanostructured LLZO using electrospinning

Although initially developed to produce ultrathin polymer fibers [66], electrospinning has become a versatile method for synthesizing a variety of ceramic nanowires through the incorporation of inorganic sols within the polymer precursor matrix. followed by calcination to remove the organic compounds and form the polycrystalline ceramic nanowires [67-69]. Similar to polymer sol-gel methods, the functional groups on the polymer are used to bind dissolved metal ions to form a gel and constrain particle nucleation and growth [70]. However, during crystallization, coalescence is further minimized due to the separation of the nanowires, with the final grain size limited by the dimensions of the nanowires. The preparation of most common binary metal oxides (e.g. TiO<sub>2</sub>, ZnO, SiO<sub>2</sub> Al<sub>2</sub>O<sub>3</sub>) using electrospinning has already been well-established, while recently, electrospinning has also been used to prepare complex oxides more relevant for battery applications [71] such as  $LiCoO_2$  [72],  $LiMn_2O_4$  [73],  $Li_4Ti_5O_{12}$  [74], Li,La(TiO<sub>3</sub>) [75,76], and the subject of this review, Li<sub>7</sub>La<sub>3</sub>Zr<sub>2</sub>O<sub>12</sub> [43,44].

A typical lab-scale electrospinning set-up [68] consists of a spinneret (e.g. a metallic needle tip), a metallic collector and a power supply, as depicted schematically in Figure 1a. Before spinning, a syringe is filled with a viscous solution containing the LLZO sol-gel/polymer precursor mixture, and the spinneret is connected to the syringe. The positive electrode of the power supply is linked to the spinneret, and the collector is connected to ground. During the spinning process, both the syringe pump and the power supply are turned on; the solution will be pushed out of the spinneret tip, forming a droplet. Since the droplet is electrified, it will experience dragging forces towards the collector exerted by the electric field, but is still balanced by the surface tension of the liquid at this stage. When the applied voltage exceeds a critical value, surface tension can no longer hold the liquid in place. The droplet will then shape into a cone (known as a Taylor cone) and a jet will shoot out from the apex. The jet is accelerated through the electric field and elongated due to the high viscosity, forming a continuous fiber that is deposited onto the collector as a mat, which can be removed as a free-standing membrane (Figure 1b-c).

In our experiments, the home-made electrospinning setup (Figure 1d) is composed of a syringe pump (New Era), a high voltage power supply (Gamma Power Supply, ES40P-20W/DAM), and a flat stationary collector made of aluminum foil. A flat-tipped

needle is installed onto a syringe and electrical connections are established to the spinneret and collector using cables with alligator clips. In a typical electrospinning experiment to prepare LLZO nanowires, the voltage is set between 7 to 11 kV; the distance between the needle tip and the collector is kept at 10 to 15 cm, and the feed rate is adjusted between 0.1 to 0.3 mL/h, depending on the type of precursor solution.

The choice of sol-gel precursors and solvent can play a role in the electrospinning conditions needed. As shown in Figure 2. several LLZO electrospinning precursors can be used. In all cases, the Li:La:Zr molar ratio is fixed at 7.7:3:2, i.e., with 10% excess Li to account for Li loss due to volatility. The LLZO sol-gel is made from lithium acetate or nitrate, lanthanum acetate or nitrate, and zirconium oxynitrate or propoxide precursors. The polymer solution is 15 wt% polyvinylpyrrolidone (PVP, Mw  $\sim$  1,300,000) in acetic acid. The acetic acid is used to stabilize the solution and control the hydrolysis of the sol-gel precursors [67]. Fortunately, the location of our laboratory is in a region (the desert Southwest of the United States) with very low average humidity and therefore no climate control chamber is needed to prevent premature hydrolysis of the sol-gel precursor during electrospinning. The LLZO aqueous sol-gel and polymer solutions are mixed at a 2:1 ratio by volume to form the electrospinning precursor, while a 1:1 ratio is used for the non-aqueous sol-gel.

For the preparation of LLZO nanowires using the aqueous precursor, we find that for the acetate-based precursors, setting the voltage to 7 kV and feed-rate to 0.12 mL/h yield the best results, while the nitrate-based precursors require a voltage of 11 kV and feed rate of 0.16 mL/h. For the non-aqueous precursor (*i.e.*, using N, N-dimethyl formamide (DMF) as solvent), a voltage of 8 kV and feed rate of 0.24 mL/h is used. Typically, the mass of the recovered LLZO nanowires after calcination is about one-fourth the mass of the as-spun nanowires when using the precursor with aqueous solvent (or one-seventh when using the non-aqueous solvent). Generally, the synthesis can be scaled up by using a multi-syringe pump, as illustrated in Figure 1e.

The choice of electrospinning precursor can affect the calcination times required to form crystalline LLZO and also the morphologies of the resulting nanowires. This can be seen in Figure 3. While the as-spun polymer fibers (Figure 3a) using the aqueous and non-aqueous precursors are very similar in morphology, the morphologies of the resulting nanowires after calcination are very different. Using a calcination temperature of 700 °C, 3 h were required to fully crystallize the nanowires obtained using the aqueous precursor [43], but the c-LLZO that was formed adopted a

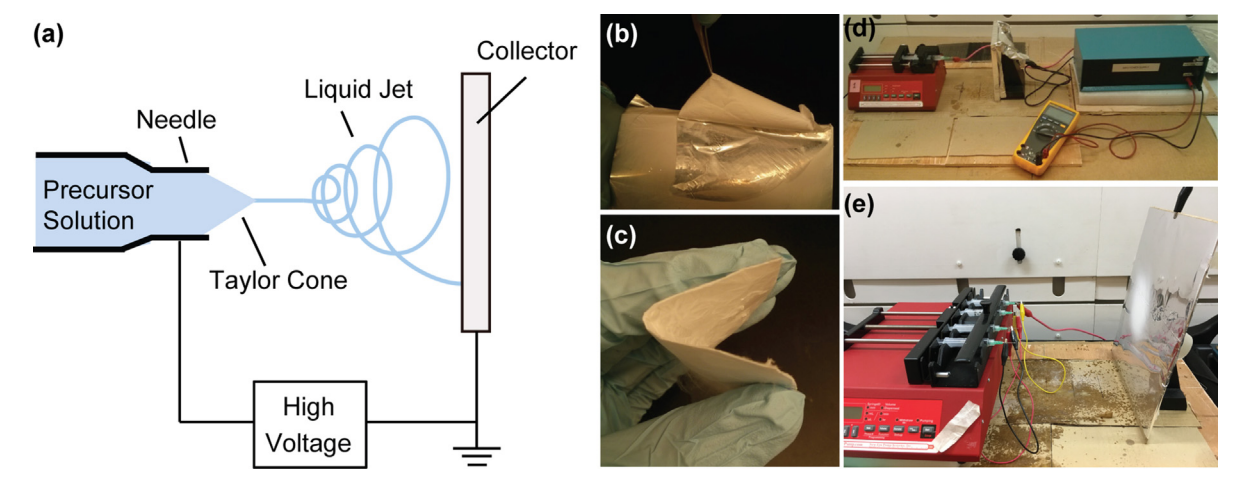


**Figure 1.** (a) Schematic setup for electrospinning; Photographs of (b) as-spun nanowire mat being removed from the collector; reprinted with permission from [76], copyright (2015) Elsevier; (c) free-standing as-spun nanowire mat; reprinted with permission from [43], copyright (2015) American Chemical Society; (d) single-syringe electrospinning setup; (e) multi-syringe electrospinning setup.

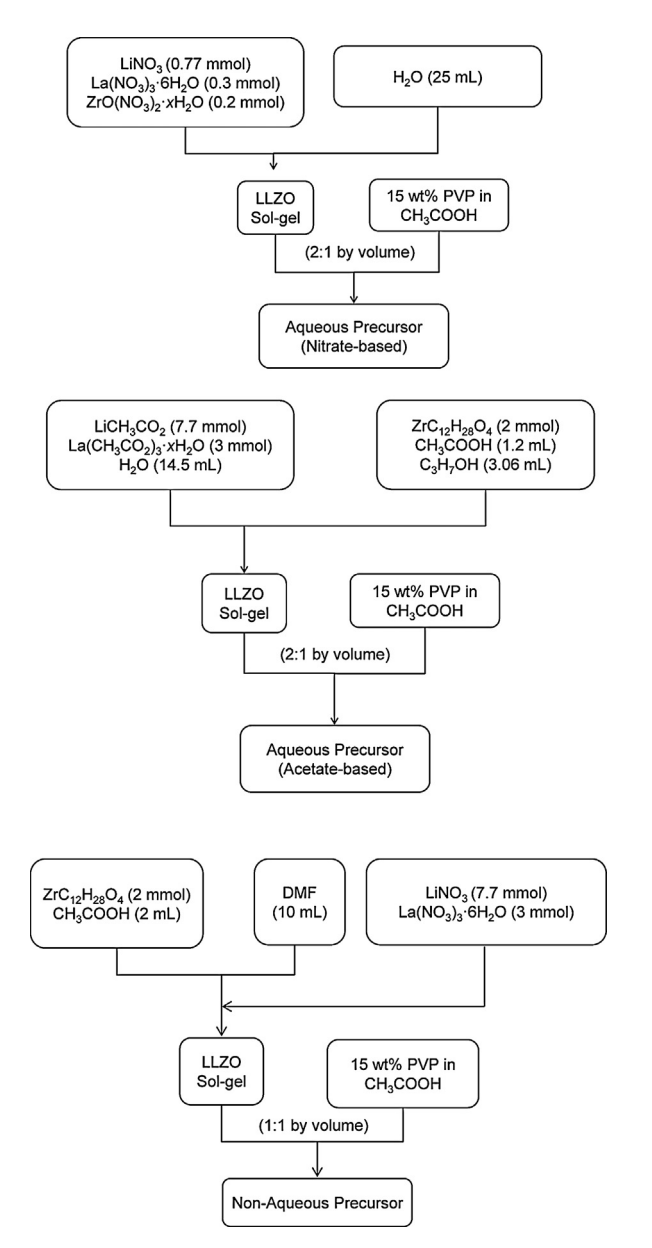


**Figure 2.** Flow chart for the preparation of aqueous and non-aqueous precursors for the electrospinning synthesis of LLZO nanowires.

morphology that can be described as interconnected "ligaments" with dimensions of 100 – 200 nm (Figure 3c). On the other hand, c-LLZO can be obtained from the nanowires electrospun from the non-aqueous precursor (Figure 3g) using only 1 h calcination at 700 °C [77]. Due to the shorter calcination time, there is also less shape change in the nanowires, although there is still a tendency to form interconnected morphologies. These morphologies arise if the nanowires are in contact with each other, since they can form junctions and merge during calcination.

The mechanism of LLZO formation from electrospun nanowires prepared using the aqueous precursor (acetate-based) was elucidated by monitoring the phase and morphology evolution during calcination at 700 °C (Figure 3a-f) [43]. With less than 2 h of calcination, the nanowires are composed of predominately La<sub>2</sub>Zr<sub>2</sub>O<sub>7</sub> nanocrystals (10 – 20 nm in size) surrounded by an amorphous shell that most likely contains lithium. The observations suggest that during the calcination process, La<sub>2</sub>Zr<sub>2</sub>O<sub>7</sub> first forms as small crystallites within the nanowire core and then reacts with the amorphous, Li-rich shell to form c-LLZO after 3 h of

calcination. As the heating time increases, the nanowires become thicker and undergo coalescence to form larger ligaments. These morphology changes are also accompanied by a phase transformation from c-LLZO to t-LLZO (Figure 3f), particularly after longer heating times (e.g. 5 h) that promote the coalescence of the ligaments to form micron-sized particles (Figure 3e). Varying the electrospinning conditions to synthesize larger diameter LLZO nanowires (Figure 3h) also revealed that the tetragonal distortion in the cubic structure could be seen in these materials, while smaller diameter nanowires adopted the c-LLZO structure (Figure 3i-j). These results point to a diameter dependence on the phase stability in electrospun LLZO nanowires, with c-LLZO found in smaller diameter nanowires and t-LLZO present in larger diameter ones.

#### 2.2. Nanostructured LLZO using cellulose templating

The preparation of metal oxides by templating onto natural cellulosic and plant-based matter has emerged as another strategy for obtaining a broad range of porous materials [78-82]. In this method, the cellulosic material can be impregnated with a solution containing the ceramic precursor (typically in the form of metal salts, but also alkoxide precursors), which is subsequently combusted to remove the organic materials and calcined to obtain the ceramic in the desired crystal structure. In other words, the formation process of the ceramic is similar to the case with electrospinning, except that pre-existing polymer fibers (the cellulose in this case) are utilized as sacrificial templates and to absorb the LLZO precursors rather than the polymer/sol fibers formed during electrospinning. Prior research on cellulosictemplated materials has shown that high surface area, nanostructured replicates with good correspondence to the original template can be obtained [78,83]. On this basis, we hypothesized that templates using nanocellulose fibers (NCF), which are the cellulose polymers found in plant cell walls with diameters ranging from 2 – 20 nm [84–86], could result in nanostructured LLZO.

When using the sol-gel reported by Janani et al. (metal nitrate salts with citric acid as chelating agent) [87] as the LLZO precursor, materials prepared by templating onto cellulose substrates show ligament-like morphologies, whereas the sol-gel calcined without a cellulose template (Figure 4a) does not [88]. It is notable that the morphologies of the final LLZO products (Figure 4c,e,g) do not show a strong correspondence to the morphologies of the starting cellulose fibers (Figure b,d,f), but rather adopt a similar interconnected morphology to the one we observed after calcination of the LLZO nanowires prepared by electrospinning [43]. This is consistent with the similar formation mechanism proceeding through the La<sub>2</sub>Zr<sub>2</sub>O<sub>7</sub> nanocrystalline intermediate phase. Further, LLZO templated onto commercial filter paper (Whatman 42) and laboratory tissue paper (Kimwipes) display larger ligament feature sizes than those templated onto NCFs (Figure 4b-g) [88]. Similar to the electrospun LLZO nanowires, a calcination temperature of 700 °C was sufficient to crystallize the LLZO precursor and remove the organic material, while heating at 800 °C tends to result in grain coalescence and formation of larger ligaments that prefer the t-LLZO phase. The NCF-templated LLZO is also characterized by fewer impurity and secondary phases (such as La(OH)<sub>3</sub>, La<sub>2</sub>O<sub>3</sub>, and La<sub>2</sub>Zr<sub>2</sub>O<sub>7</sub>, which indicate insufficient mixing and/or degree of reaction) than the other templates (Figure 4h-j). Hence, from these results, LLZO prepared by templating on NCF can offer more phase pure materials adopting the c-LLZO structure at room temperature without requiring extrinsic dopants.

These observations further support the size-dependent formation of c-LLZO that we observed in our electrospinning synthesis of undoped c-LLZO nanowires. We also found that c-LLZO particles  $\sim$ 

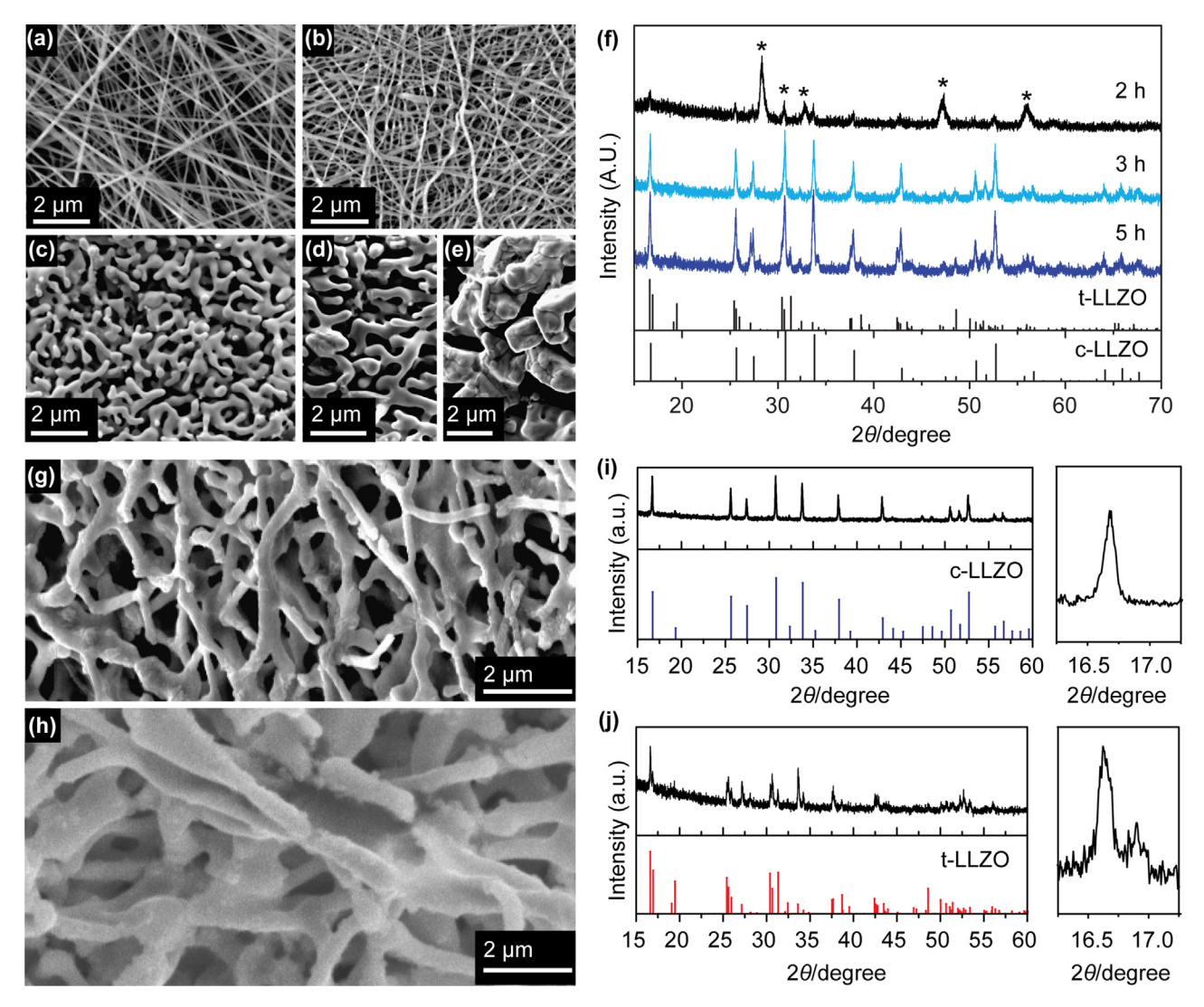


Figure 3. Electrospun LLZO nanowires from aqueous precursor. Scanning electron microscopy (SEM) image of (a) as-spun LLZO/polymer nanowires and the nanowires after calcination at  $700^{\circ}$ C for (b) 2 h, (c) 3 h, (d) & (e) 5 h. (f) X-ray diffraction (XRD) patterns showing the effect of calcination time on the product. (\*) La<sub>2</sub>Zr<sub>2</sub>O<sub>7</sub>. Electrospun nanowires from non-aqueous precursor after calcination at  $700^{\circ}$ C. SEM images of nanowires with average diameter of (g) 276 nm after calcination for 1 h, and (h) 477 nm after calcination for 2 h. Corresponding XRD patterns are shown in (i) and (j), respectively. The zoom-in of the reflection shows the larger diameter nanowires adopted the t-LLZO structure while the smaller diameter nanowires are c-LLZO. (a) – (f) Reproduced and adapted with permission from [43], copyright (2015) American Chemical Society.

25 nm in size could be prepared by ball-milling bulk t-LLZO [43]. Many other groups have also reported observations of the cubic phase in undoped LLZO calcined at low temperatures, which subsequently transformed to t-LLZO at higher temperatures. The tendency for researchers to use extrinsic dopants to form c-LLZO and lack of consistency in reporting particle sizes or microscopy images make it difficult to perform a full survey on the particle-size dependency of cubic phase formation in c-LLZO from the literature. However, in the next section we attempt to highlight those methods using low temperature calcinations (< 900 °C) to obtain nano-sized LLZO, particularly those that also report c-LLZO in undoped materials.

### 2.3. Nanostructured LLZO using other low temperature methods

A number of research groups have applied conventional sol-gel methods for the preparation of LLZO. These methods (e.g. Pechini, modified Pechini, polymer complex, etc.) are regularly used to obtain a variety of nanostructured ceramics [70]. LLZO prepared using a conventional sol-gel method (using metal nitrates, citric acid, and ethylene glycol) followed by calcination at 800 °C, was

found to adopt the t-LLZO structure, but no particle size information was provided and lower calcination temperatures were not explored [89]. Kokal *et al.* used a modified, aluminumfree Pechini method to prepare LLZO and found that after heating at 700 °C, c-LLZO with a particle size of 300 - 500 nm was formed, but calcination at 800 °C caused the particle sizes to increase to 500 - 1000 nm and changed the structure to tetragonal [90]. In the study by Xie *et al.*, aluminum-free c-LLZO nanoparticles ~20 nm in size that aggregated into particles ~10  $\mu$ m in size were obtained by precipitating the acetate salts in acetic acid followed by calcination at 750 °C; the powders were found to decompose to La<sub>2</sub>Zr<sub>2</sub>O<sub>7</sub> above 800 °C [91].

One of the advantages of sol-gel based methods is that the addition of dopants is usually straightforward due to the homogenous mixing of the precursors. For instance, addition of aluminum nitrate to the sol-gel precursor is effective for preparing Al-doped, c-LLZO [92]. A "hybrid sol-gel" approach [93] was developed where solid precursors of LLZO and Al $_2$ O $_3$  were prepared using sol-gel methods at 900 °C and 750 °C, respectively. The formed Al $_2$ O $_3$  was amorphous but displayed a nanosheet morphology, with thickness of 50 – 100 nm and width of several

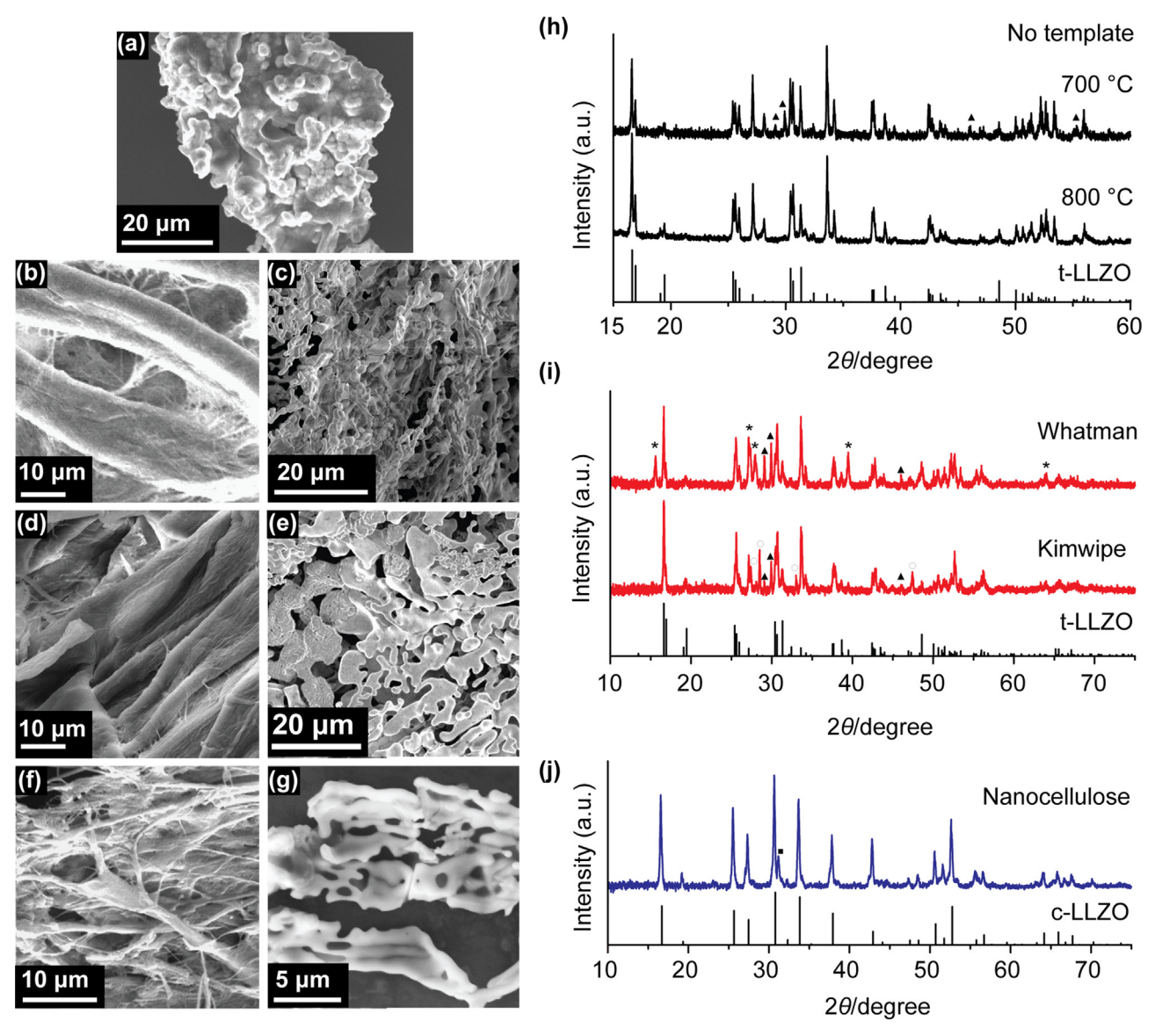


Figure 4. Undoped LLZO synthesized by templating sol-gel precursors onto cellulose substrates. SEM images of (a) LLZO sol-gel calcined without a cellulose template; as-obtained templates (b) Whatman 42 filter paper, (d) Kimwipes paper, (f) nanocellulose fibers; (c),(e), and (g) show the corresponding templated LLZO after calcination. XRD patterns of (h) LLZO sol-gel calcined without a cellulose template at 700 °C for 5 h or 800 °C for 12 h to yield t-LLZO; (i) LLZO templated onto Whatman 42 and Kimwipe templates after calcination for 800 °C for 12 h, (j) LLZO templated onto nanocellulose fibers after calcination for 800 °C for 12 h. (\*) La(OH)<sub>3</sub>; (▲) La<sub>2</sub>O<sub>3</sub>; (∘) La<sub>2</sub>Zr<sub>2</sub>O<sub>7</sub>; (■) unidentified impurity. Reproduced and adapted with permission from [88], copyright (2016) American Chemical Society.

microns. The two solid precursors were then co-sintered to form a dense pellet at 1100 °C for only 3 h, while Al-doped LLZO sintered at the same conditions could not be fully densified. The improved densification behavior and more homogenous Al3+ incorporation in the Al-doped LLZO prepared using this hybrid sol-gel approach is attributed due to the high surface area and amorphous nature of the  $Al_2O_3$  nanosheets, as well as the *in situ* formation of LiAlO<sub>2</sub>, which acted to reduce Li<sup>+</sup> volatilization and also may have served as a sintering aid [93]. Afyon et al. also reported improved densification in Ga-doped c-LLZO nanoparticles 200 - 300 nm in size synthesized by calcining t-LLZO particles with Ga<sub>2</sub>O<sub>3</sub> [94]. The t-LLZO particles (300 nm - 1 µm in size) were prepared using a modified sol-gel combustion method that avoided the use of carboxylic acids and ethylene glycol so that lower temperatures and shorter calcination times could be used, with t-LLZO obtained at only 600 °C and pellets with bulk Li<sup>+</sup> conductivity of  $\sim$ 4.0  $\times$  10<sup>-4</sup> S cm<sup>-1</sup> at 20 °C obtained after sintering at 950 °C for only 6 h.

Sakamoto *et al.* reported a sol-gel synthesis involving the mixture of a zirconium alkoxide chelated by acetic acid with a separate solution containing lithium, lanthanum, and aluminum (as dopant) salts to form a gel with extensive metal-oxygen bonding [61]. Supercritical drying of the gel revealed an aerogel morphology consisting of a highly interconnected solid network with  $\sim \! 10 \, \mathrm{nm}$  wide nanowire-like crosslinks, surface area of 292  $\mathrm{m^2/g}$ , and large fraction of microporosity (33%). Unfortunately, this supercritically dried gel was not calcined or studied further, but conventional drying of the gel revealed that the LLZO could be obtained after heat treatment in an argon environment. This is attributed to the metal-oxygen bonds formed during the gelation period, in contrast to Pechini based methods, where heating in air is required to provide sufficient oxygen to form the crystallized ceramic.

Co-precipitation methods have also been effective for synthesizing LLZO. A wet co-precipitation method, wherein a mixed hydroxide precursor was prepared by mixing the metal nitrates

with an alkaline solution, resulted in LLZO with a plate-like morphology with lengths of 300 - 600 nm and widths of 50 -100 nm after calcination at 700 °C; the particles became more spherical and increased in size as the calcination temperature increased, with t-LLZO (and other impurity phases) observed after calcination at 900 °C [95]. Another co-precipitation approach [96] used ammonium carbonate as precipitant to make flaky La<sub>3</sub>Z $r_2Al_{0.25}CO_3/OH$  particles < 1 micron in size: this precipitate was subsequently coated with a lithium oxalate  $(Li_2C_2O_4)$  shell <100 nm thick. This core-shell structure was calcined and c-LLZO was formed starting at 700 °C, but with co-existence of La<sub>2</sub>Zr<sub>2</sub>O<sub>7</sub>, via LaCO<sub>3</sub>(OH) and Li<sub>2</sub>C<sub>2</sub>O<sub>4</sub> phases that were observed at 500 °C. Pure phase, Al-doped c-LLZO was obtained after calcination at 900 °C. The particle sizes of the obtained c-LLZO were not provided, but the grain sizes of the LaCO<sub>3</sub>(OH) and Li<sub>2</sub>C<sub>2</sub>O<sub>5</sub> intermediate phases were calculated to be 66.8 nm and 51 nm, respectively, using the Scherrer equation. A two-step approach was also used by Kumar et al. [97] by creating a precursor via ball-milling of ZrO<sub>2</sub> nanoparticles with La(OH)<sub>3</sub> and AlOOH, followed by impregnation of the powder mixture with lithium acetate. Pure phase c-LLZO was obtained after calcination at 750°C, with crystallite size of 135.8 nm determined using the Scherrer equation and average particle size of 90 nm from dynamic light scattering (DLS) measurements. However, scanning electron microscopy (SEM) imaging revealed that the particles were agglomerated into larger particles 1 - 2 microns in size.

Yi et al. found that flexible, Al or Ga-doped c-LLZO thin films < 30 µm thick could be prepared from a liquid-feed flame spray pyrolysis approach [98,99]. In this method, nanopowders were prepared by aerosolizing a solution of lithium propionate. lanthanum isobutyrate, zirconium isobutyrate, and alumatrane [Al(OCH<sub>2</sub>CH<sub>2</sub>)<sub>3</sub>N] or gallium-atrane [Ga(OCH<sub>2</sub>CH<sub>2</sub>)<sub>3</sub>N] with oxygen followed by combustion in an oxidizing flame. The obtained powders were spherical nanoparticles with average size of 90 nm, but were composed of Li<sub>2</sub>CO<sub>3</sub> and off-stoichiometric La<sub>2</sub>Zr<sub>2</sub>O<sub>7</sub> rather than LLZO [98]. The authors attribute the formation of these "decomposed LLZO" nanoparticles to the high flame temperatures > 1500 °C and presence of H<sub>2</sub>O and CO<sub>2</sub> as combustion byproducts. Interestingly, dense c-LLZO thin films (94 - 95% relative density) could still be obtained from these particles with pressure-less sintering using much shorter heating times than is typically required for bulk LLZO (only 1 h sintering at 1090°C for Al-LLZO and 0.3 h at 1130 °C for Ga-LLZO), with the improved densification attributed to the uniform packing and high surface energy of the nanoparticles, as well as liquid phase sintering facilitated by the presence of Li<sub>2</sub>CO<sub>3</sub>. Additionally, the authors proposed that Li<sup>+</sup>/H<sup>+</sup> exchange on the surface of the nanoparticles could actually improve sintering through reaction driven densification of the decomposed LLZO [99]. These studies show that nanomaterials comprised of intermediate phases or constituent oxides of LLZO can also provide a promising route towards obtaining LLZO solid electrolytes.

# 3. Application of nanostructured LLZO as ceramic fillers in polymer electrolytes

3.1. Nanostructured LLZO as ceramic fillers in PEO-based composite polymer electrolytes (CPEs)

Polymer composite electrolytes (CPEs) are emerging as a promising compromise between solid polymer electrolytes (which suffer from poor mechanical properties and low room temperature conductivities) [100,101] and pellet-type ceramic electrolytes (which are brittle, display interface issues, and are difficult to process) [17]. CPEs composed of polymer electrolytes embedded with ceramic particles comprising inert or "passive" materials (i.e., displaying no intrinsic Li<sup>+</sup> ion conductivity) can be designed to show improvements in both conductivity and mechanical properties compared to the individual components [102-105]. In these cases, the ceramic filler generally serves to increase the highly conducting amorphous regions in crystalline polymers such as polyethylene oxide (PEO). Recently, the use of "active" materials, (i.e., ceramic or glassy materials that also display Li<sup>+</sup> ionic conductivity) has attracted interest due to the potential of the CPE to display synergistic properties, with much interest lately in using LLZO as the ceramic filler.

So far, CPEs containing LLZO have predominately employed PEO in the polymer matrix, with either LiClO<sub>4</sub> or lithium bis (trifluoromethanesulfonyl)imide (LiTFSI) as the Li<sup>+</sup> salt. PEO-based polymer electrolytes typically display low ionic conductivities ( $\sim 10^{-5} - 10^{-8}$  S cm<sup>-1</sup> between 35 – 65 °C) due to the low mobility of Li<sup>+</sup> through the crystalline regions of the PEO [106]. The introduction of plasticizers comprising passive, nano-sized ceramic particles (*e.g.* SiO<sub>2</sub>, Al<sub>2</sub>O<sub>3</sub>, TiO<sub>2</sub>) can enable faster Li<sup>+</sup> transport and improve the ionic conductivity to >  $10^{-4}$  S cm<sup>-1</sup> in the composites [106,107]. However, when using active fillers (*e.g.*, the Li<sup>+</sup> conducting ceramic Li<sub>1.3</sub>Al<sub>0.3</sub>Ti<sub>1.7</sub>(PO<sub>4</sub>)<sub>3</sub>, LATP), larger particles (0.5 – 1.5  $\mu$ m) have also been effective for improving the ionic conductivity in the CPE [108].

On the other hand, results from studies using LLZO particles as ceramic fillers in PEO suggest that micron-sized fillers may not be effective. Langer et~al. investigated PEO-based CPEs with ceramic fillers consisting of Al-doped c-LLZO particles (up to  $\sim 5$  microns in size, BET surface area 0.52  $m^2~g^{-1}$ ) prepared by co-precipitation [109]. The CPE containing 40 vol% of LLZO displayed an ionic conductivity of  $5\times 10^{-5}~S~cm^{-1}$  at  $80\,^{\circ}\text{C}$ , which was comparable to

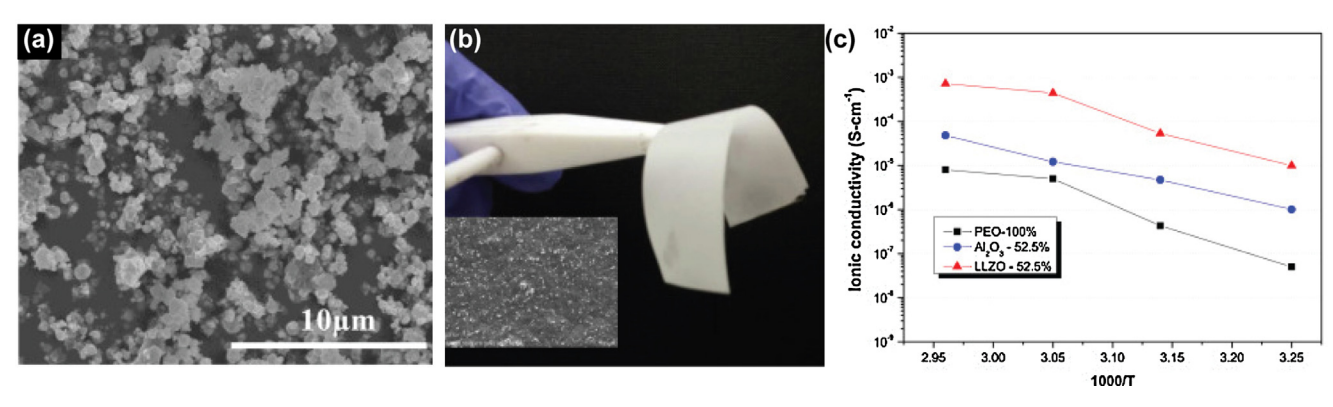


Figure 5. SEM image of t-LLZO prepared using Pechini-type sol-gel; (b) photo and SEM image (inset) of the CPE membrane containing 52.5% LLZO in PEO/LiClO<sub>4</sub> polymer matrix; (c) ionic conductivity of membranes with respect to temperature. Reproduced and adapted with permission from [112], copyright (2015) Elsevier.

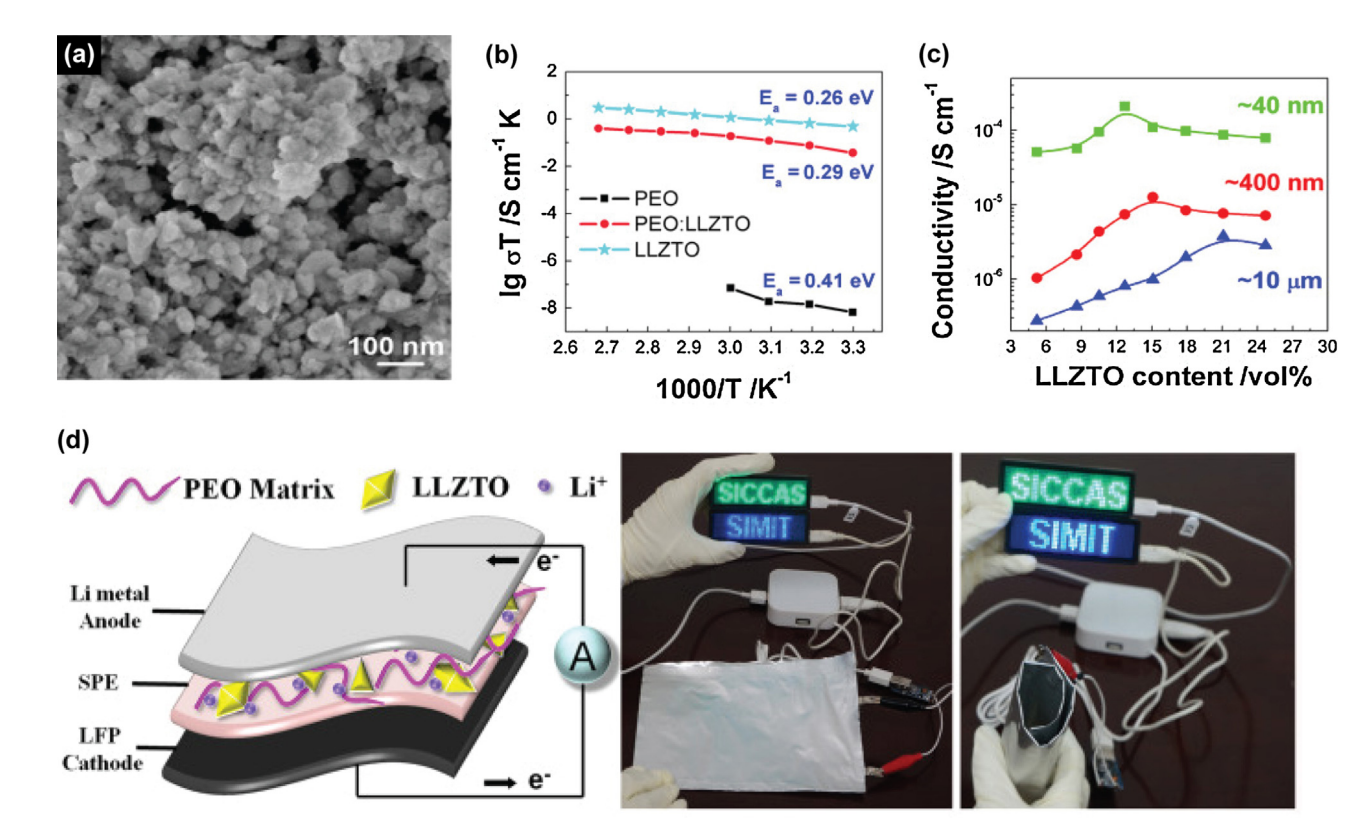
the conductivity of a LLZO pellet at that temperature, but the CPE conductivity was much lower ( $\sim 10^{-9}~S~cm^{-1}$ ) at  $20~^\circ C$ . The authors speculated that there may have been an insulating  $\text{Li}_2\text{CO}_3$  coating on the LLZO, which forms upon exposure of LLZO to humid air and has been shown to lead to high interfacial impedance [110]. Since the Li $^+$  concentration within LLZO was one order of magnitude higher than in the polymer, the authors also proposed that Li ions may have diffused from the LLZO to the PEO to balance the concentration gradient, which would have decreased the LLZO ionic conductivity.

The CPEs reported by Keller et al. also displayed lower ionic conductivity ( $\sim 10^{-5}$  S cm<sup>-1</sup> at room temperature) than pure LLZO and the LLZO-free polymer matrix [111]. In this work, the c-LLZO filler particles ( $D_{50} = 0.9 \mu m$ ) were used at 70 wt% in PEO/LiTFSI membranes using solvent-free processing in an attempt to prevent the LLZO from reacting with ambient air and to avoid the formation of surface carbonates and hydroxides. The authors proposed that the incorporation of LLZO into the CPE may have increased the tortuosity in the pathways for Li<sup>+</sup> transport, leading to a decrease in conductivity. The possibility of grain boundary resistance between LLZO particles and presence of interfacial resistance between the LLZO and polymer matrix were also suggested to affect the Li<sup>+</sup> diffusion. Despite the lower ionic conductivity, the interfacial resistance of the CPE in contact w/Li metal was decreased compared to the polymer or LLZO alone. Hence, if the polymer/ ceramic interfacial resistances are addressed to improve the ionic transport, such CPEs may serve as promising solid electrolytes for Li metal batteries.

The LLZO fillers used by Choi *et al.* [112] were prepared using a conventional Pechini-type polymer complex method and adopted the t-LLZO structure with 0.5  $\mu m < D_{50} < 1~\mu m)$  (Figure 5a ). The maximum ionic conductivity of  $\sim 10^{-5}~S~cm^{-1}$  at 35 °C was found in PEO/LiClO<sub>4</sub> CPEs containing 52.5% LLZO (Figure 5b), which was two

orders of magnitude higher than that for a membrane of PEO/LiClO<sub>4</sub> alone or one using Al<sub>2</sub>O<sub>3</sub> as filler (Figure 5c). That the CPE ionic conductivity displayed a synergistic effect is particularly interesting considering that t-LLZO, which is intrinsically less conducting than the c-LLZO used in the work by Langer *et al.* [109] and Keller *et al.*[111], was used as the filler. It is not clear if this result arises due to the smaller particle size of the t-LLZO fillers. The t-LLZO-based CPE also displayed electrochemical stability from 0 – 5 V vs. Li/Li<sup>+</sup>, as well as better kinetics and improved charge/discharge efficiency in a cell with a Li metal anode and LiNi<sub>0.6</sub>Co<sub>0.2</sub>Mn<sub>0.2</sub>O<sub>2</sub> cathode compared to a comparison membrane containing 52.5 wt% Al<sub>2</sub>O<sub>3</sub> [112].

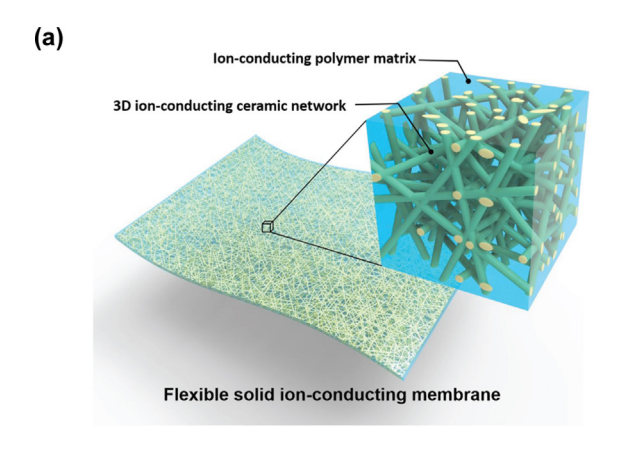
Zhang et al. further extended the ceramic filler concept to the nanoscale by using Ta-doped c-LLZO (LLZTO) with average particle size of  $\sim 40\,\mathrm{nm}$  (Figure 6a) [113]. The LLZO nanoparticles were prepared from ~10 µm LLZTO particles using planetary ballmilling, followed by high-energy ball-milling under the protection of argon. The authors prepared CPEs of LLZTO with PEO only (i.e., without an additional Li<sup>+</sup> salt). Interestingly, the authors found that the ionic conductivity in the CPEs was still quite high despite the insulating nature of the Li<sup>+</sup> salt-free PEO, with the maximum ionic conductivity of  $2.1 \times 10^{-4}$  S cm<sup>-1</sup> (30 °C) observed when using 12.7 vol% of LLZTO nanoparticles as fillers, compared to only  $3.8 \times 10^{-6}$  S cm<sup>-1</sup> using 10  $\mu$ m LLZTO particles at 21.1 vol% and 1.3  $\times$  10<sup>-5</sup> S cm<sup>-1</sup> using 400 nm LLZTO nanoparticles at 15.1 vol% (Figure 6b-c). The authors suggest that the Li<sup>+</sup> transport mechanism is through highly conductive paths that are formed at the LLZTO/PEO interface, and that some of the Li<sup>+</sup> can also be transferred from the LLZTO to the PEO. The particle-size dependent results (Figure 6c) are consistent with a percolation effect on the ionic conductivity enhancement. with different percolation thresholds for the different particle sizes and higher conductivity in the nanoparticle-embedded CPEs due to the higher surface-to-volume ratio of the fillers. Further, extended

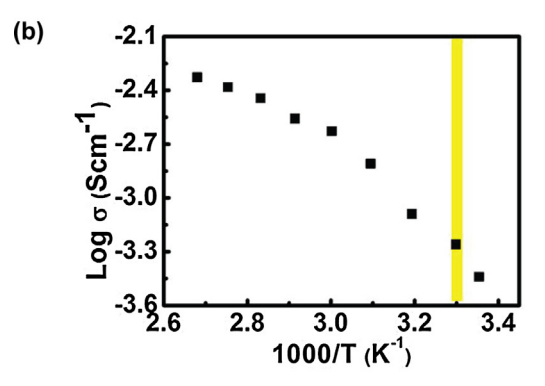


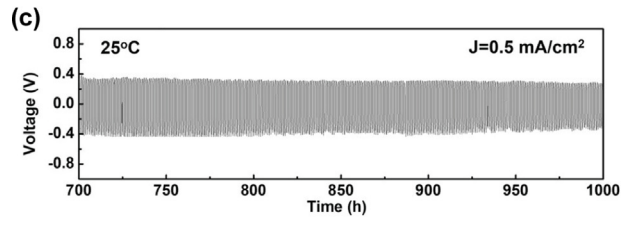
**Figure 6.** (a) SEM image of LLZTO nanoparticles; (b) Arrhenius plots of the PEO, PEO/LLZTO CPE with 12.7 vol% LLZTO, and LLZTO pellets; (c) The conductivity as a function of LLZTO volume fraction for the LLZTO particles with different sizes; (d) Schematic and photographs of flexible pouch cell using SPE, LiFePO<sub>4</sub> (LFP) as cathode, and Li metal anode. Reproduced and adapted with permission from [113], copyright (2016) Elsevier.

cycling with Li metal electrodes showed that compared to CPEs prepared from LLZTO/PEO/LiTFSI CPEs, the LLZTO/PEO CPEs were more stable to Li metal dendrite growth. This is attributed to the formation of better, more homogenous interfaces with the Li metal electrodes and absence of Li<sup>+</sup> transport in the insulating PEO regions. Flexible, all-solid-state Li metal batteries (Figure 6d) prepared using LiFePO<sub>4</sub>-based cathodes displayed good rate capability and cycling performance, showing that the nano-LLZO embedded CPEs operating on interfacial transport at the LLZO/polymer interface may be a promising solution for high performance batteries.

In the work by Fu *et al.*, Al-doped c-LLZO nanowires (average diameter of 138 nm) prepared by electrospinning were used as nanostructured ceramic fillers for PEO-based CPEs [44]. The nanowire mat directly obtained after electrospinning was calcined and then a PEO/LiTFSI solution was infiltrated into the empty space within the three-dimensional LLZO network in order to create a "fiber-reinforced" CPE with extended interfaces between the LLZO and PEO (Figure 7a). With an approximate LLZO filler loading of 20 wt%, the resulting CPEs displayed excellent thermal stability, room temperature ionic conductivity of  $2.5 \times 10^{-4}$  S cm<sup>-1</sup> (Figure 7b),

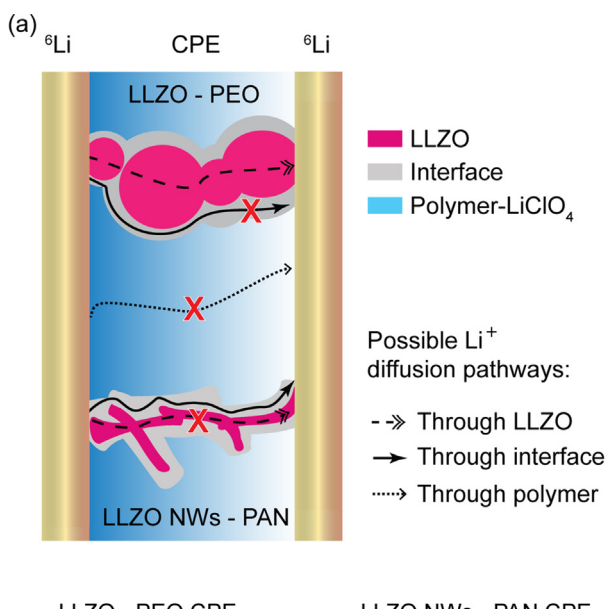






**Figure 7.** (a) Schematic of LLZO nanowire reinforced composite polymer electrolyte; (b) Arrhenius plot of CPE from 20 – 90 °C; (c) Voltage profile of continuous lithium plating/stripping with a current density of 0.5 mA cm<sup>-2</sup> at 25 °C. Reproduced and adapted with permission from [44]; copyright (2016) National Academy of Sciences.

stable voltage window up to 6.0 V vs. Li/Li<sup>+</sup>, and were effective for blocking lithium dendrite formation during repeated lithium stripping/plating at 0.5 mA cm<sup>-2</sup> for 1,000 h (Figure 7c). The impressive properties of these CPEs was attributed to the creation of continuous, long-range ion transport pathways through the use of the interconnected LLZO nanowire network as the filler, but the Li<sup>+</sup> transport pathways were not empirically verified.



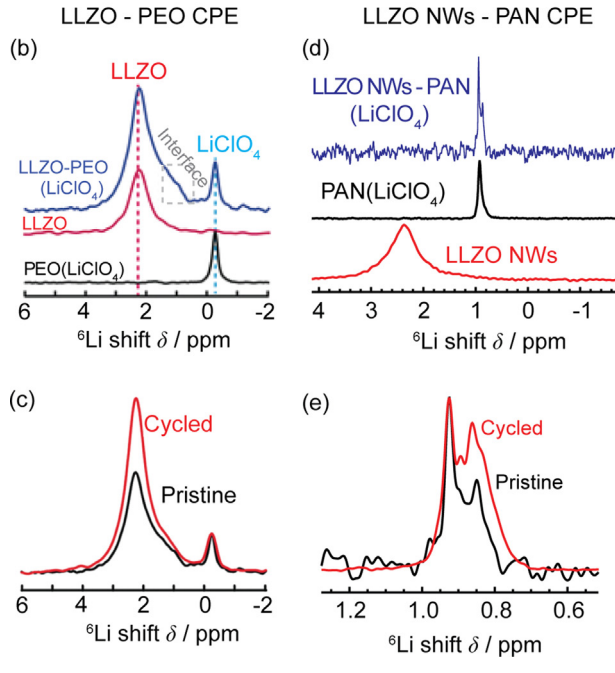


**Figure 8.** (a) Schematic showing possible Li\* transport pathways in CPE made from LLZO in PEO and LLZO nanowires (NWs) in PAN with LiClO<sub>4</sub> as the salt in both cases. The "X" shows pathways that are not preferred, according to the solid-state Li NMR results. <sup>6</sup>Li NMR spectra to identify Li local environments in the CPE and each individual component: (b) <sup>6</sup>Li NMR spectra of CPE, PEO/LiClO<sub>4</sub>, and LLZO particles; (c) Comparison of <sup>6</sup>Li spectra of LLZO/PEO/LiClO<sub>4</sub> CPE before (pristine) and after cycling in <sup>6</sup>Li foil symmetric cells. (d) <sup>6</sup>Li NMR spectra of CPE, PAN/LiClO<sub>4</sub>, and LLZO NWs; (e) Comparison of <sup>6</sup>Li spectra of LLZO NWs/PAN/LiClO<sub>4</sub> CPE before (pristine) and after cycling in <sup>6</sup>Li foil symmetric cells. (b),(c) are reproduced with permission from [114], copyright (2016) Wiley; (d),(e) are reproduced and adapted with permission from [77], copyright (2017) American Chemical Society.

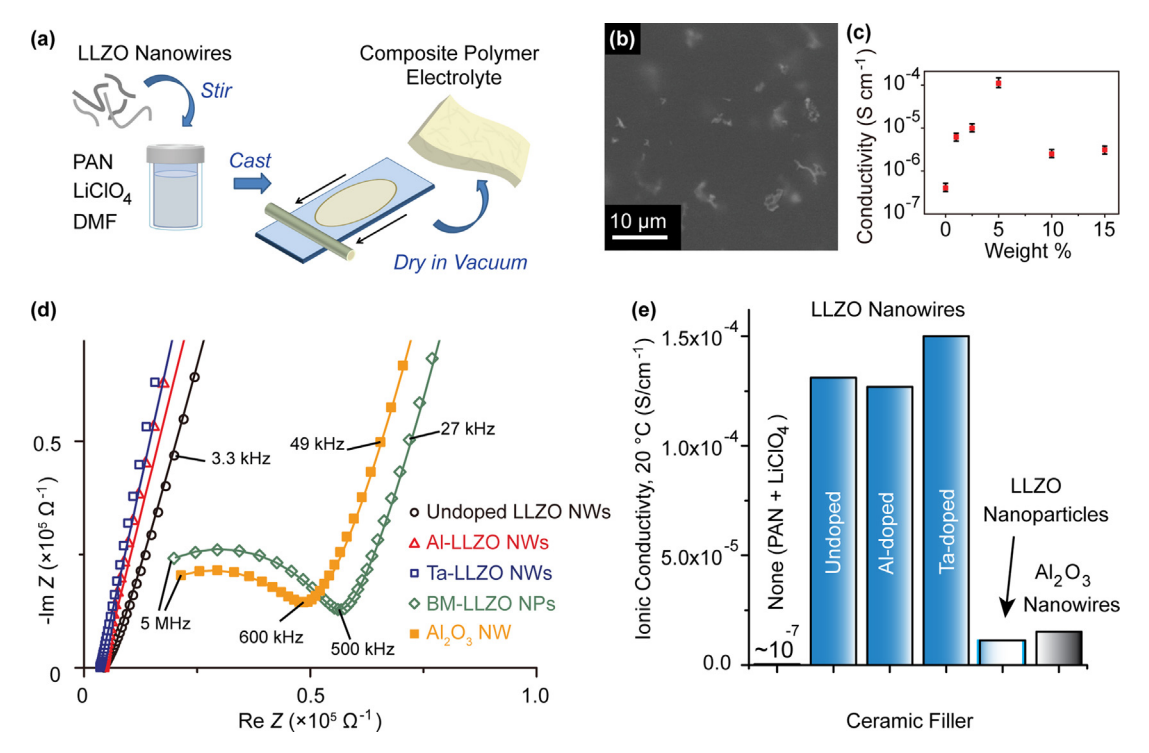


**Figure 9.** (a) Schematic procedure to prepare CPE from LiClO<sub>4</sub>/polyacrylonitrile (PAN) matrix with LLZO nanowire fillers; (b) SEM image of a CPE film; (c) Ionic conductivity comparison at 20 °C of CPEs embedded with different wt% of undoped LLZO NWs, with the conductivity of a blank sample for reference. Each point is the average of three measurements and the error bars indicate the standard deviation; (d) Representative Nyquist plots and (e) ionic conductivity of CPEs embedded with 5 wt% of different filler materials, all tested at 20 °C. (b) – (e) Reproduced with permission from [77], copyright (2017) American Chemical Society.

## 3.2. Analysis of ${\rm Li}^{\star}$ transport pathways in LLZO-based CPEs using nuclear magnetic resonance

The aforementioned studies show how the design of highly conducting electrolytes could be improved through better understanding of the mechanism of Li<sup>+</sup> transport within the CPEs. In general, Li<sup>+</sup> diffusion can take place through the polymer matrix phase, through the LLZO filler phase, or through the interfacial regions (Figure 8a). As mentioned before, the Li<sup>+</sup> transport can be hindered by crystalline regions in the PEO, the presence of insulating surface coatings on the LLZO, or a grain boundary resistance between LLZO particles. In the event where the percolation threshold for the LLZO filler is not met, an interfacial resistance between LLZO and the polymer matrix may also affect Li<sup>+</sup> diffusion.

Zheng et al. developed a method to determine the preferred Li<sup>+</sup> pathways in CPEs using solid-state Li nuclear magnetic resonance (NMR) measurements and a <sup>6</sup>Li-<sup>7</sup>Li isotope-replacement strategy [114]. First, high resolution <sup>6</sup>Li NMR spectra are obtained for the ceramic filler alone, the polymer matrix alone, and then the CPE in order to identify the Li<sup>+</sup> ions in the different local environments. Next, symmetric <sup>6</sup>Li foil/CPE/<sup>6</sup>Li foil cells are assembled and galvanostatically cycled, followed by acquisition of the <sup>6</sup>Li NMR spectra. The method builds on the basis that <sup>6</sup>Li replaces <sup>7</sup>Li during the galvanostatic cycling, and that changes in the <sup>6</sup>Li amount in the CPE before and after electrochemical cycling will reveal which Li<sup>+</sup> transport pathways are preferred. Zheng et al. found that for CPEs consisting of 50 wt% Al-doped LLZO particles in a PEO/LiClO<sub>4</sub> matrix, a resonance at -0.2 ppm from LiClO<sub>4</sub> within the PEO matrix, one at 2 ppm for Li<sup>+</sup> in c-LLZO, and a shoulder at around 1.4 ppm assigned to Li<sup>+</sup> at the PEO/LLZO interface could be identified in the <sup>6</sup>Li NMR spectrum of the CPE (Figure 8b). By comparing the <sup>6</sup>Li NMR spectrum of the pristine (uncycled) CPE with the one after galvanostatic cycling, it was evident that the resonance associated with Li<sup>+</sup> in LLZO significantly increased in intensity (Figure 8c). This indicates that Li<sup>+</sup> was found to transport preferentially through the LLZO phase, suggesting that LLZO needs to be at a high enough volume fraction to form a percolating network. These results are consistent with the fact that most LLZO/PEO CPEs contain fairly high fractions of LLZO in order to reach peak ionic conductivity.

In contrast, our studies on CPEs prepared using electrospun c-LLZO nanowires embedded into polyacrylonitrile (PAN) paint a different picture [77]. We found that by incorporating only 5 wt% (2 vol%) of LLZO nanowires by dispersion into the polymer matrix solution (Figure 9a-b), the room temperature ionic conductivity of a PAN-LiClO<sub>4</sub>-based CPE was increased 3 orders of magnitude to  $1.31 \times 10^{-4}$  S cm<sup>-1</sup> (Figure 9c). Undoped, Al-doped, and Ta-doped LLZO nanowires were utilized as fillers, but the conductivity enhancement was similar (Figure 9d-e). Additionally, the CPEs containing LLZO nanowires displayed superior ionic conductivity at 5 wt% of filler compared to those containing the same fraction of LLZO nanoparticles or Al<sub>2</sub>O<sub>3</sub> nanowire fillers (Figure 9d-e). Unlike PEO-based CPEs, where ceramic fillers act as plasticizers and enhance Li<sup>+</sup> transport through amorphous PEO regions [106], PAN films containing Li<sup>+</sup> salts are amorphous so the introduction of ceramic fillers does not significantly change the crystallinity of the polymer [75,115]. Instead, LLZO NW fillers could improve the ionic conductivity of the PAN-based CPE by increasing the Li+ dissociation from the ClO<sub>4</sub><sup>-</sup> anion, which would increase the concentration of free Li<sup>+</sup> in the CPE [116-118].

Performing solid-state NMR measurements using the same method developed by Zheng *et al.* showed that LLZO NWs partially modified the PAN polymer matrix [77]. As shown in Figure 8d, the only <sup>6</sup>Li resonances found in the CPE were that for the LiClO<sub>4</sub> in PAN at 0.90 ppm, and a new one observed at 0.85 ppm, which was attributed to LiClO<sub>4</sub> within PAN with a local structural environment modified by the LLZO nanowires. The <sup>6</sup>Li resonance from Li<sup>+</sup> in the LLZO nanowires was not observed in the CPE, presumably because of the low vol% of the LLZO in the CPE. After cycling, the resonance at 0.85 ppm increased in intensity, suggesting that Li<sup>+</sup>

diffusion is preferentially through these modified regions at the LLZO/PAN interface.

From the publications reviewed in this section, it is clear that there are numerous parameters to explore in order to engineer highly conducting LLZO filler-based CPEs. In the future, systematic investigation of the type of Li<sup>+</sup> salt and polymer in the matrix, wt% of salt and LLZO filler, composition and structure of LLZO (e.g. cubic or tetragonal, doped or undoped, presence of surface layers such as Li<sub>2</sub>CO<sub>3</sub>, etc.), and morphology of LLZO (e.g. micron or nano-sized particles, nanowires) combined with detailed, mechanistic studies and advanced characterization techniques may lead to important new insights on the required characteristics to obtain CPEs with high Li<sup>+</sup> ionic conductivity. In addition, several interesting observations regarding other properties of the CPEs, such as the improved interfacial behavior with Li metal [111,113] and better resistance to Li dendrite propagation [44,77,113], have already been reported but not fully explained. Further, studies on mechanical and thermal properties of the CPEs and long-term cycling stability are also needed.

#### 4. Conclusions and Outlook

In this review, we summarized progress in the research of nanostructured garnet-type LLZO solid electrolytes. While several methods for preparing LLZO nanomaterials have already been demonstrated, the study of the properties of nanostructured LLZO is still in its infancy. Additionally, most of the low-temperature methods for LLZO have relied on conventional sol-gel approaches, while more sophisticated colloidal chemistry methods used by the nanochemistry community have not been explored. Hydrothermal and solvothermal type methods for LLZO have also not been reported. So far, electrospinning has been demonstrated to be a robust method for preparing polycrystalline LLZO nanowires after very short heat treatments (e.g., 700 °C for 1 h using a non-aqueous precursor).

Through our own studies on the synthesis of nanostructured LLZO, we have discovered a size-dependence in the phase stability of LLZO that could potentially be exploited as an alternative route for obtaining the cubic phase of LLZO without using extrinsic doping. Similar observations are reported by other groups, but there is a lack of consistency in reporting particle sizes or microscopy images in the community. More well-controlled synthetic routes are needed to better understand size-dependent properties of LLZO, with careful monitoring of grain size, particle size, crystal structure, and composition.

In the past few years, several promising examples of LLZO as ceramic fillers in polymer composite electrolytes have already been demonstrated. To fully exploit LLZO to enhance the ionic conductivity in these CPEs, the properties of the LLZO and the polymer matrix must be carefully designed. Better understanding of the Li<sup>+</sup> diffusion pathways through the composite films, for example using <sup>6</sup>Li NMR analysis, can greatly assist the development of these electrolytes.

#### Acknowledgements

The authors gratefully acknowledge support from the NSF CAREER award DMR 1553519.

#### References

- R. Spotnitz, J. Franklin, Abuse behavior of high-power, lithium-ion cells, J. Power Sources 113 (2003) 81–100.
- [2] Q. Wang, P. Ping, X. Zhao, G. Chu, J. Sun, C. Chen, Thermal runaway caused fire and explosion of lithium ion battery, J. Power Sources 208 (2012) 210–224.

- [3] R.A. Leising, M.J. Palazzo, E.S. Takeuchi, K.J. Takeuchi, A study of the overcharge reaction of lithium-ion batteries, J. Power Sources 97–98 (2001) 681–683
- [4] T. Ohsaki, T. Kishi, T. Kuboki, N. Takami, N. Shimura, Y. Sato, M. Sekino, A. Satoh, Overcharge reaction of lithium-ion batteries, J. Power Sources 146 (2005) 97–100.
- [5] Z. Li, J. Huang, B.Y. Liaw, V. Metzler, J. Zhang, A review of lithium deposition in lithium-ion and lithium metal secondary batteries, J. Power Sources 254 (2014) 168–182.
- [6] K.N. Wood, M. Noked, N.P. Dasgupta, Lithium metal anodes: toward an improved understanding of coupled morphological, electrochemical, and mechanical behavior, ACS Energy Lett. 2 (2017) 664–672.
- [7] P.G. Balakrishnan, R. Ramesh, T.P. Kumar, Safety mechanisms in lithium-ion batteries, J. Power Sources 155 (2006) 401–414.
- [8] J.B. Goodenough, Y. Kim, Challenges for rechargeable Li batteries, Chem. Mater. 22 (2010) 587–603.
- [9] P. Knauth, Inorganic solid Li ion conductors: an overview, Solid State Ionics 180 (2009) 911–916.
- [10] J.W. Fergus, Ceramic and polymeric solid electrolytes for lithium-ion batteries, J. Power Sources 195 (2010) 4554–4569.
- [11] N.J. Dudney, Glass and ceramic electrolytes for lithium and lithium-ion batteries, in: G.A. Nazri, G. Pistoia (Eds.), Lithium Batteries – Science and Technology, Springer, New York, 2003, pp. 624–642.
- [12] C. Sun, J. Liu, Y. Gong, D.P. Wilkinson, J. Zhang, Recent advances in all-solid-state rechargeable lithium batteries, Nano Energy 33 (2017) 363–386.
- [13] R. Chen, W. Qu, X. Guo, L. Li, F. Wu, The pursuit of solid-state electrolytes for lithium batteries: from comprehensive insight to emerging horizons, Mater. Horiz, 3 (2016) 487–516.
- [14] B.D. McCloskey, Attainable gravimetry and volumetric energy density of Li-S and Li ion battery cells with solid separator-protected Li metal anodes, J. Phys. Chem. Lett. 6 (2015) 4581–4588.
- [15] G. Girishkumar, B. McKloskey, A.C. Luntz, S. Swanson, W. Wilcke, Lithium-air battery: promise and challenges, J. Phys. Chem. Lett. 1 (2010) 2193–2203.
- [16] K. Hayashi, Y. Nemeto, S. Tobishima, J. Yamaki, Electrolyte for high voltage Li/ LiMn<sub>1.9</sub>Co<sub>0.1</sub>O<sub>4</sub>, J. Power Sources. 68 (1997) 316–319.
- [17] K. Kerman, A. Luntz, V. Viswanathan, Y.M. Chiang, Z. Chen, Review Practical challenges hindering the development of solid state Li ion batteries, J. Electrochem. Soc. 164 (2017) A1731–A1744.
- [18] Y. Inaguma, C. Liquan, M. Itoh, T. Nakamura, High ionic conductivity in lithium lanthanum titanate, Solid State Communications 86 (1993) 693–698.
- [19] C.H. Chen, K. Amine, Ionic conductivity, lithium insertion and extraction of lanthanum lithium titanate, Solid State Ionics 144 (2001) 51–57.
- [20] K.Y. Yang, I.C. Leu, K.Z. Fung, M.S. Hon, M.C. Hsu, Y.J. Hsiao, M.C. Wang, Mechanism of the interfacial reaction between cation-deficient La<sub>0.56</sub>Li<sub>0.33</sub>TiO<sub>3</sub> and metallic lithium at room temperature, J. Mater. Res. 23 (2008) 1813–1825.
- [21] V. Thangadurai, H. Kaack, W. Weppner, Novel fast lithium ion conduction in garnet-type Li<sub>5</sub>La<sub>3</sub>M<sub>2</sub>O<sub>12</sub> (M = Nb, Ta), J. Am. Ceram. Soc. 86 (2003) 437–440.
- [22] R. Murugan, V. Thangadurai, W. Weppner, Fast lithium ion conduction in garnet-type Li<sub>7</sub>La<sub>3</sub>Zr<sub>2</sub>O<sub>12</sub>, Angew. Chem. Int. 46 (2007) 7778–7781.
- [23] V. Thangadurai, S. Narayanan, D. Pinzaru, Garnet-type solid-state fast Li ion conductors for Li batteries: critical review, Chem. Soc. Rev. 43 (2014) 4714– 4727
- [24] S. Teng, J. Tan, A. Tiwari, Recent developments in garnet based solid state electrolytes for thin film batteries, Curr. Opin. Solid St. M. 18 (2014) 29–38.
- [25] S. Ramakumar, C. Deviannapoorani, L. Dhivya, L.S. Shankar, R. Murugan, Lithium garnets: synthesis, structure, Li<sup>+</sup> conductivity, Li<sup>+</sup> dynamics and applications, Prog. Mater. Sci. 88 (2017) 325–411.
- [26] N. Bernstein, M.D. Johannes, K. Hoang, Origin of the structural phase transition in Li<sub>7</sub>La<sub>3</sub>Zr<sub>2</sub>O<sub>12</sub>, Phys. Rev. Lett. 109 (2012) 205702.
- [27] J. Awaka, N. Kijima, H. Hayakawa, J. Akimoto, Synthesis and structure of tetragonal Li<sub>7</sub>La<sub>3</sub>Zr<sub>2</sub>O<sub>12</sub> with the garnet-related type structure, J. Solid State Chem. 182 (2009) 2046–2062.
- [28] E.A. Il'ina, O.L. Andreev, B.D. Antonov, N.N. Batalov, Morphology and transport properties of the solid electrolyte Li<sub>7</sub>La<sub>3</sub>Zr<sub>2</sub>O<sub>12</sub> prepared by the solid-state and citrate-nitrate methods, J. Power Sources 201 (2012) 169–173.
- [29] C.A. Geiger, E. Alekseev, B. Lazi, M. Fisch, T. Armbruster, R. Langner, M. Fechtelkord, N. Kim, T. Pettke, W. Weppner, Crystal chemistry and stability of "Li<sub>2</sub>La<sub>3</sub>Zr<sub>2</sub>O<sub>12</sub>" garnet: a fast lithium-ion conductor, Inorg. Chem. 50 (2011) 1089–1097.
- [30] M. Matsui, K. Takahashi, K. Sakamoto, A. Hirano, Y. Takeda, O. Yamamoto, N. Imanishi, Phase stability of a garnet-type lithium ion conductor Li<sub>7</sub>La<sub>3</sub>Zr<sub>2</sub>O<sub>12</sub>, Dalton Trans. 43 (2014) 1019–1023.
- [31] T. Logéat, U. Köhler, B. Eisele, A. Stiaszny, M. Harzer, A. Tovar, H. Senyshyn, B. Ehrenberg, Kozinsky, From order to disorder: the structure of lithium-conducting garnets Li<sub>7-x</sub>La<sub>3</sub>Ta<sub>x</sub>Zr<sub>2-x</sub>O<sub>12</sub> (x = 0-2), Solid State Ionics 206 (2012) 33–38.
- [32] D. Rettwenwander, G. Redhammer, F. Preishuber-Pflüg, L. Cheng, L. Miara, R. Wagner, A. Welzl, E. Suard, M.M. Doeff, M. Wilkening, J. Fleig, G. Amthauer, Structural and electrochemical consequences of Al and Ga cosubstitution in Li<sub>7</sub>La<sub>3</sub>Zr<sub>2</sub>O<sub>12</sub> solid electrolytes, Chem. Mater. 28 (2016) 2384–2392.
- [33] J.F. Wu, W.K. Pang, V.K. Peterson, L. Wei, X. Guo, Garnet-type fast Li-ion conductors with high ionic conductivities for all-solid-state batteries, ACS Appl. Mater. Interfaces 9 (2017) 12461–12468.
- [34] G. Larraz, A. Orera, M.L. Sanjuán, Cubic phases of garnet-type  $\text{Li}_7\text{La}_3\text{Zr}_2\text{O}_{12}$ : the role of hydration, J. Mater. Chem. A 1 (2013) 11419–11428.

- [35] Y. Wang, W. Lai, Phase transition in lithium garnet oxide ionic conductors Li<sub>7</sub>La<sub>3</sub>Zr<sub>2</sub>O<sub>12</sub>; the role of Ta substitution and H<sub>2</sub>O/CO<sub>2</sub> exposure, J. Power Sources 275 (2015) 612–620.
- [36] E. Rangasamy, J. Wolfenstine, J. Sakamoto, The role of Al and Li concentration on the formation of cubic garnet solid electrolyte of nominal composition Li<sub>7</sub>La<sub>3</sub>Zr<sub>2</sub>O<sub>12</sub>, Solid State Ionics 206 (2012) 28–32.
- [37] R.C. Garvie, Stabilization of the tetragonal structure in zirconia microcrystals, J. Phys. Chem. 82 (1978) 218–224.
- [38] H. Zhang, J.F. Banfield, Thermodynamic analysis of phase stability of nanocrystalline titania, J. Mater. Chem. 8 (1998) 2073–2076.
- [39] A. Navrotsky, Energetics of nanoparticle oxides: interplay between surface energy and polymorphism, Geochem. Trans. 4 (2003) 34–37.
- [40] A. Navrotsky, Energetics at the nanoscale: impacts for geochemistry, the environment, and materials, MRS Bulletin 41 (2016) 139–145.
- [41] S. Toda, K. Ishiguro, Y. Shimonishi, A. Hirano, Y. Takeda, O. Yamamoto, N. Imanishi, Low temperature cubic garnet-type CO<sub>2</sub>-doped Li<sub>7</sub>La<sub>3</sub>Zr<sub>2</sub>O<sub>12</sub>, Solid State Ionics 233 (2013) 102–106.
- [42] I. Quinzeni, D. Capsoni, V. Berbenni, P. Mustarelli, M. Sturini, M. Bini, Stability of low-temperature Li<sub>7</sub>La<sub>3</sub>Zr<sub>2</sub>O<sub>12</sub> cubic phase: the role of temperature and atmosphere, Mater. Chem. Phys. 185 (2017) 55–64.
- [43] T. Yang, Z.D. Gordon, Y. Li, C.K. Chan, Nanostructured garnet-type solid electrolytes for lithium batteries: electrospinning synthesis of Li<sub>7</sub>La<sub>3</sub>Zr<sub>2</sub>O<sub>12</sub> nanowires and particle size-dependent phase transformation, J. Phys. Chem. C 119 (2015) 14947–14953.
- [44] K. Fu, Y. Gong, J. Dai, A. Gong, X. Han, Y. Yao, C. Wang, Y. Wang, Y. Chen, C. Yan, Y. Li, E.D. Wachsman, L. Hu, Flexible, solid-state, ion-conducting membrane with 3D garnet nanofiber networks for lithium batteries, Proc, Natl. Acad. Sci. USA 113 (2016) 7094–7099.
- [45] T. Liu, Y. Ren, Y. Shen, S.X. Zhao, Y. Lin, C.W. Nan, Achieving high capacity in bulk-type solid-state lithium ion battery based on Li<sub>6.75</sub>La<sub>3</sub>Zr<sub>1.75</sub>Ta<sub>0.25</sub>O<sub>12</sub> electrolyte: interfacial resistance, J. Power Sources 324 (2016) 349–357.
- [46] F. Yonemoto, A. Nishimura, M. Motoyama, N. Tsuchimine, S. Kobayashi, Y. Iriyama, Temperature effects on cycling stability of Li plating/stripping on Tadoped Li<sub>7</sub>La<sub>3</sub>Zr<sub>2</sub>O<sub>12</sub>, J. Power Sources 343 (2017) 207–215.
- [47] R.H. Basappa, T. Ito, H. Yamada, Contact between garnet-type solid electrolyte and lithium metal anode: influence on charge transfer resistance and short circuit prevention, J. Electrochem. Soc. 154 (2017) A666–A671.
- [48] C.L. Tsai, V. Roddatis, C.V. Chandran, Q. Ma, S. Uhlenbruck, M. Bram, P. Heitjans, O. Guillon, Li<sub>7</sub>La<sub>3</sub>Zr<sub>2</sub>O<sub>12</sub> interface modification for Li dendrite prevention, ACS Appl. Mater. Interfaces 8 (2016) 10617–10626.
- [49] J. van den Broek, S. Afyon, J.L.M. Rupp, Interface-engineered all-solid-state Liion batteries based on garnet-type fast Li\* conductors, Adv. Energy Mater. 6 (2016) 1600736.
- [50] X. Han, Y. Gong, K. Fu, X. He, G.T. Hitz, J. Dai, A. Pearse, B. Liu, H. Wang, G. Rubloff, Y. Mo, V. Thangadurai, E.D. Wachsman, L. Hu, Negating interfacial impedance in garnet-based solid-state Li metal batteries, Nature Mater. 16 (2017) 572–579.
- [51] C. Wang, Y. Gong, B. Liu, K. Fu, Y. Yao, E. Hitz, Y. Li, J. Dai, S. Xu, W. Luo, E.D. Wachsman, L. Hu, Conformal, nanoscale ZnO surface modification of garnet-based solid-state electrolytes for lithium metal anodes, Nano Lett. 17 (2017) 565–571.
- [52] B. Liu, Y. Gong, K. Fu, X. Han, Y. Yao, G. Pastel, C. Yang, H. Xie, E.D. Wachsman, L. Hu, Garnet solid electrolyte protected Li-metal batteries, ACS Appl. Mater. Interfaces 9 (2017) 18809–18815.
- [53] K.H. Kim, Y. Iriyama, K. Yamamoto, S. Kumazaki, T. Asaka, K. Tanabe, C.A.J. Fisher, T. Hirayama, R. Murugan, Z. Ogumi, Characterization of the interface between LiCoO<sub>2</sub> and Li<sub>2</sub>La<sub>3</sub>Zr<sub>2</sub>O<sub>12</sub> in an all-solid-state rechargeable lithium battery, J. Power Sources 196 (2011) 764–767.
- [54] K. Park, B.C. Yu, J.W. Jung, Y. Li, W. Zhou, H. Gao, S. Son, J.B. Goodenough, Electrochemical nature of the cathode interface for a solid-state lithium-ion battery: interface between LiCoO<sub>2</sub> and garnet-Li<sub>7</sub>La<sub>3</sub>Zr<sub>2</sub>O<sub>12</sub>, Chem. Mater. 28 (2016) 8051–8059.
- [55] Y. Ren, T. Liu, Y. Shen, Y. Lin, C.W. Nan, Chemical compatibility between garnet-like solid state electrolyte Li<sub>6.75</sub>La<sub>3</sub>Zr<sub>1.75</sub>Ta<sub>0.25</sub>O<sub>12</sub> and major commercial lithium battery cathode materials, J. Materiomics 2 (2016) 256– 264
- [56] Y. Ren, Y. Shen, Y. Lin, C.W. Nan, Direct observation of lithium dendrites inside garnet-type lithium-ion solid electrolyte, Electrochem. Commun. 57 (2015) 27–30
- [57] A. Sharafi, H.M. Meyer, J. Nanda, J. Wolfenstine, J. Sakamoto, Characterizing the Li-  $\text{Li}_7\text{La}_3\text{Zr}_2\text{O}_{12}$  interface stability and kinetics as a function of temperature and current density, J. Power Sources 302 (2016) 135–139.
- [58] E.J. Cheng, A. Sharafi, J. Sakamoto, Intergranular Li metal propagation through polycrystalline Li<sub>6.25</sub>Al<sub>0.25</sub>La<sub>3</sub>Zr<sub>2</sub>O<sub>12</sub> ceramic electrolyte, Electrochim. Acta 223 (2017) 85–91.
- [59] L. Cheng, C.H. Wu, A. Jarry, W. Chen, Y. Ye, J. Zhu, R. Kostecki, K. Persson, J. Guo, M. Salmeron, G. Chen, M. Doeff, Interrelationships among grain size, surface composition, air stability, and interfacial resistance of Al-substituted Li<sub>7</sub>La<sub>3</sub>Zr<sub>2</sub>O<sub>12</sub> solid electrolytes, ACS Appl. Mater. Interfaces 7 (2015) 17649–17655.
- [60] L. Cheng, W. Chen, M. Kunz, K. Persson, N. Tamura, G. Chen, M. Doeff, Effect of surface microstructure on electrochemical performance of garnet solid electrolytes, ACS Appl. Mater. Interfaces 7 (2015) 2073–2081.
- [61] J. Sakamoto, E. Rangasamy, H. Kim, Y. Kim, J. Wolfenstine, Synthesis of nanoscale fast ion conducting cubic Li<sub>7</sub>La<sub>3</sub>Zr<sub>2</sub>O<sub>12</sub>, Nanotechnology 24 (2013) 424005.

- [62] J.R. Groza, Nanosintering, Nanostructured Materials 12 (1999) 987-992.
- [63] Z.Z. Fang, H. Wang, X. Wang, V. Kumar, Grain growth during sintering of nanosized particles, in: R.K. Bordia, E.A. Olevsky (Eds.), Advances in Sintering Science and Technology: Ceramic Transations, Wiley, Hoboken, 2010, pp. 389–400.
- [64] P. Bowen, C. Carry, From powders to sintered pieces: forming, transformations and sintering of nanostructured ceramic oxides, Powder Technology 128 (2002) 248–255.
- [65] M.J. Mayo, Superplasticity of nanostructured ceramics, in: M. Nastasi, D. Parkin, H. Gleiter (Eds.), Mechanical Properties and Deformation Behavior of Materials Having Ultra-Fine Microstructures. vol. 233, Ch. IV, Springer, Dordrecht, 1993, pp. 361–380.
- [66] C.J. Luo, S.D. Stoyanov, E. Stride, E. Pelan, M. Edirisinghe, Electrospinning versus fibre production methods: from specifics to technological convergence, Chem. Soc. Rev. 41 (2012) 4708–4735.
- [67] D. Li, Y. Xia, Fabrication of titania nanofibers by electrospinning, Nano Lett. 3 (2003) 555–560.
- [68] D. Li, J.T. McCann, Y. Xia, Electrospinning: a simple and versatile technique for producing ceramic nanofibers and nanotubes, J. Am. Ceram. Soc. 89 (2006) 1861–1869.
- [69] R. Ramaseshan, S. Sundarrajan, R. Jose, S. Ramakrishna, Nanostructured ceramics by electrospinning, J. Appl. Phys. 102 (2007) 111101.
- [70] A.E. Danks, S.R. Hall, Z. Schnepp, The evolution of 'sol-gel' chemistry as a technique for materials synthesis, Mater. Horizons 3 (2016) 91–112.
- [71] H.G. Wang, S. Yuan, D.L. Ma, X.B. Zhang, J.M. Yan, Electrospun materials for lithium and sodium rechargeable batteries: from structure evolution to electrochemical performance, Energy Environ. Sci. 8 (2015) 1660–1681.
- [72] C. Shao, N. Yu, Y. Liu, R. Mu, Preparation of LiCoO<sub>2</sub> nanofibers by electrospinning technique, J. Phys. Chem. Solids 67 (2006) 1423–1426.
- [73] N. Yu, C. Shao, Y. Liu, H. Guan, X. Yang, Nanofibers of LiMn<sub>2</sub>O<sub>4</sub> by electrospinning, J. Colloid Interf. Sci. 285 (2005) 163–166.
- [74] N. Zhu, W. Liu, M. Xue, Z. Xie, Z. Xie, D. Zhao, M. Zhang, J. Chen, T. Cao, Graphene as a conductive additive to enhance the high-rate capabilities of electrospun Li<sub>4</sub>Ti<sub>5</sub>O<sub>12</sub> for lithium-ion batteries, Electrochim. Acta 55 (2010) 5813–5818.
- [75] W. Liu, N. Liu, J. Sun, P.C. Hsu, Y. Li, H.W. Lee, Y. Cui, Ionic conductivity enhancement of polymer electrolytes with ceramic nanowire fillers, Nano Lett. 15 (2015) 2740–2745.
- [76] T. Yang, Y. Li, C.K. Chan, Enhanced lithium ion conductivity in lithium lanthanum titanate solid electrolyte nanowires prepared by electrospinning, J. Power Sources 287 (2015) 164–169.
- [77] T. Yang, J. Zheng, Q. Cheng, Y.Y. Hu, C.K. Chan, Composite polymer electrolytes with Li<sub>7</sub>La<sub>3</sub>Zr<sub>2</sub>O<sub>12</sub> garnet-type nanowires as ceramic fillers: mechanism of conductivity enhancement and role of doping and morphology, ACS Appl. Mater. Interfaces 9 (2017) 21773–21780.
- [78] J. Huang, T. Kunitake, Nano-precision replication of natural cellulosic substances by metal oxides, J. Am. Chem. Soc. 125 (2003) 11834–11835.
- [79] J.H. Schattka, E.H.M. Wong, M. Antonietti, R.A. Caruso, Sol-gel templating of membranes to form thick, porous titania, titania/zirconia and titania/silica films, J, Mater. Chem. 16 (2006) 1414–1420.
- [80] P. Greil, Templating approaches using natural cellular plant tissue, MRS Bull. 35 (2010) 145–149.
- [81] D. Van Opdenbosch, G. Zollfrank, Cellulose-based biotemplated silica structuring, Adv. Eng. Mater. 16 (2014) 699–712.
  [82] X. Deng, C.K. Chan, H. Tüysüz, Spent tea leaf templating of cobalt-based
- [82] X. Deng, C.K. Chan, H. Tuysuz, Spent tea leaf templating of cobalt-based mixed oxide nanocrystals for water oxidation, ACS Appl. Mater. Interfaces 8 (2016) 32488–32495.
- [83] A.N. Shigapov, G.W. Graham, R.W. McCabe, H.K. Plummer, Preparation of high-surface area, thermally-stable, metal-oxide catalysts and supports by a cellulose templating approach, Appl. Catal. A - Gen. 210 (2001) 287–300.
- [84] W. Stelte, A.R. Sanadi, Preparation and characterization of cellulose nanofibers from two commercial hardwood and softwood pulps, Ind. Eng. Chem. Res. 48 (2009) 11211–11219.
- [85] C. Salas, T. Nypelö, C. Rodriguez-Abreu, C. Carrillo, O.J. Rojas, Nanocellulose properties and applications in colloids and interfaces, Curr. Opin. Colloid. In. 19 (2014) 383–396.
- [86] J.H. Kim, B.S. Shim, H.S. Kim, Y.J. Lee, S.K. Min, D. Jang, Z. Abas, J. Kim, Review of nanocellulose for sustainable future materials, Int. J. Precis. Eng. Man. 2 (2015) 197–213.
- [87] N. Janani, S. Ramakumar, L. Dhivya, C. Deviannapoorani, K. Saranya, R. Murugan, Synthesis of cubic Li<sub>7</sub>La<sub>3</sub>Zr<sub>2</sub>O<sub>12</sub> by modified sol-gel process, lonics 17 (2011) 575–580.
- [88] Z.D. Gordon, T. Yang, G.B.G. Morgado, C.K. Chan, Preparation of nano- and microstructured garnet Li<sub>7</sub>La<sub>3</sub>Zr<sub>2</sub>O<sub>12</sub> solid electrolytes for Li-ion batteries via cellulose templating, ACS Sustainable Chem. Eng. 4 (2016) 6391–6398.
- [89] Y. Shimonishi, A. Toda, T. Zhang, A. Hirano, N. Imanishi, O. Yamamoto, Y. Takeda, Synthesis of garnet-type Li<sub>7-x</sub>La<sub>3</sub>Zr<sub>2</sub>O<sub>12-1/2x</sub> and its stability in aqueous solutions, Solid State Ionics 183 (2011) 48–53.
- [90] I. Kokal, M. Somer, P.H.L. Notten, H.T. Hintzen, Sol-gel synthesis and lithium ion conductivity of Li<sub>7</sub>La<sub>3</sub>Zr<sub>2</sub>O<sub>12</sub> with garnet-related type structure, Solid State Ionics 185 (2011) 42–46.
- [91] X. Xie, Y. Li, J.B. Goodenough, Low-temperature synthesis of Li<sub>7</sub>La<sub>3</sub>Zr<sub>2</sub>O<sub>12</sub> with cubic garnet-type structure, Mater. Res. Bull. 47 (2012) 1229–1232.
- [92] Y. Jin, P.J. McGinn, Al-doped Li<sub>7</sub>La<sub>3</sub>Zr<sub>2</sub>O<sub>12</sub> synthesized by a polymerized complex method, J. Power Sources 196 (2011) 8683–8687.

- [93] H. El-Shinawi, G.W. Paterson, D.A. MacLaren, E.J. Cussen, S.A. Corr, Low-temperature densification of Al-doped Li<sub>7</sub>La<sub>3</sub>Zr<sub>2</sub>O<sub>12</sub>: a reliable and controllable synthesis of fast-ion conducting garnets, J. Mater. Chem. A 5 (2017) 319–329.
- [94] S. Afyon, F. Krumeich, J.L.M. Rupp, A shortcut to garnet-type fast Li-ion conductors for all-solid state batteries, J. Mater. Chem. A 3 (2015) 18636– 18648
- [95] K.W. Kim, S.H. Yang, M.Y. Kim, M.S. Lee, J. Lim, D.R. Chang, H.S. Kim, Cubic phase behavior and lithium ion conductivity of Li<sub>7</sub>La<sub>2</sub>Zr<sub>2</sub>O<sub>12</sub> prepared by coprecipitation synthesis for all-solid batteries, J. Ind. Eng. Chem. 36 (2016) 279–283.
- [96] Y. Zhang, J. Cai, F. Chen, R. Tu, Q. Shen, X. Zhang, L. Zhang, Preparation of cubic Li<sub>7</sub>La<sub>3</sub>Zr<sub>2</sub>O<sub>12</sub> solid electrolyte using a nano-sized core-shell structured precursor, J. Alloys Compounds 644 (2015) 709–793.
- [97] P.J. Kumar, K. Nishimura, M. Senna, A. Düvel, P. Heitjans, T. Kawaguchi, N. Sakamoto, N. Wakiya, H. Suzuki, A novel low-temperature solid-state route for nanostructured cubic garnet Li<sub>7</sub>La<sub>3</sub>Zr<sub>2</sub>O<sub>12</sub> and its application to Li-ion battery, RSC Adv. 6 (2016) 62656–62667.
- [98] E. Yi, W. Wang, J. Kieffer, R.M. Laine, Flame made nanoparticles permit processing of dense, flexible, Li<sup>+</sup> conducting ceramic electrolyte thin films of cubic-Li<sub>7</sub>La<sub>3</sub>Zr<sub>2</sub>O<sub>12</sub> (c-LLZO), J. Mater. Chem. A 4 (2016) 12947–12954.
- [99] E. Yi, W. Wang, J. Kieffer, R.M. Laine, Key parameters governing the densification of cubic-Li<sub>7</sub>La<sub>3</sub>Zr<sub>2</sub>O<sub>12</sub> Li<sup>+</sup> conductors, J. Power Sources 352 (2017) 156–164.
- [100] W.H. Meyer, Polymer electrolytes for lithium-ion batteries, Adv. Mater. 10 (1998) 439-448.
- [101] R.C. Agrawal, G.P. Pandey, Solid polymer electrolytes: materials designing and all-solid-state battery applications: an overview, J. Phys. D: Appl. Phys. 41 (2008) 223001.
- [102] X. Fu, D. Yu, J. Zhou, S. Li, X. Gao, Y. Han, P. Qi, X. Feng, B. Wang, Inorganic and organic hybrid solid electrolytes for lithium-ion batteries, CrystEngComm 18 (2016) 4236–4258.
- [103] M.M.É. Jacob, E. Hackett, E.P. Giannelis, From nanocomposite to nanogel polymer electrolytes, J. Mater. Chem 13 (2003) 1–5.
- [104] S. Kalnaus, A.S. Sabau, W.E. Tenhaeff, N.J. Dudney, C. Daniel, Design of composite polymer electrolytes for Li ion batteries based on mechanical stability criteria, J. Power Sources 201 (2012) 280–287.
- [105] S.H. Kim, K.H. Choi, S.J. Cho, E.H. Kil, S.Y. Lee, Mechanically compliant and lithium dendrite growth-suppressing composite polymer electrolytes for flexible lithium-ion batteries, J. Mater. Chem. A 1 (2013) 4949–4955.
- [106] F. Croce, G.B. Appetecchi, L. Persi, B. Scrosati, Nanocomposite polymer electrolytes for lithium batteries 1998 (2015) 456–458.

- [107] F. Croce, R. Curini, A. Martinelli, L. Persi, F. Ronci, B. Scrosati, R. Caminiti, Physical and chemical properties of nanocomposite polymer electrolytes, J. Phys. Chem. 1999 (2017) 10632–10638.
- [108] Y.J. Wang, Y. Pan, D. Kim, Conductivity studies on ceramic Li<sub>1.3</sub>Al<sub>0.3</sub>Ti<sub>1.7</sub>(PO<sub>4</sub>)<sub>3</sub>filled PEO-based solid composite polymer electrolytes, J. Power Sources 159 (2006) 690–701.
- [109] F. Langer, I. Bardenhagen, J. Glenneberg, R. Kun, Microstructure and temperature dependent lithium ion transport of ceramic-polymer composite electrolyte for solid-state lithium ion batteries based on garnettype Li<sub>7</sub>La<sub>3</sub>Zr<sub>2</sub>O<sub>12</sub>, Solid State Ionics 291 (2016) 8–13.
- [110] L. Cheng, E.J. Crumlin, W. Chen, R. Qiao, H. Hou, S.F. Lux, V. Zorba, R. Russo, R. Kostecki, Z. Liu, K. Persson, W. Yang, J. Cabana, T. Richardson, G. Chen, M. Doeff, The origin of high electrolyte electrode interfacial resistances in lithium cells containing garnet type solid electrolytes, Phys. Chem. Chem. Phys. 16 (2014) 18294–18300.
- [111] M. Keller, G.B. Appetecchi, G.T. Kim, V. Sharova, M. Schneider, J. Schuhmacher, A. Roters, S. Passerini, Electrochemical performance of a solvent-free hybrid ceramic-polymer electrolyte based on Li<sub>7</sub>La<sub>3</sub>Zr<sub>2</sub>O<sub>12</sub> in P(EO)<sub>15</sub>LïTFSI, J. Power Sources 353 (2017) 287–297.
- [112] J.H. Choi, C.H. Lee, J.H. Yu, C.H. Doh, S.M. Lee, Enhancement of ionic conductivity of composite membranes for all-solid-state lithium rechargeable batteries incorporating tetragonal Li<sub>7</sub>La<sub>3</sub>Zr<sub>2</sub>O<sub>12</sub> into a polyethylene matrix, J. Power Sources 2015 (2017) 458–463.
- [113] J. Zhang, N. Zhao, M. Zhang, Y. Li, P.K. Chu, X. Guo, Z. Di, X. Wang, H. Li, Flexible and ion-conducting membrane electrolytes for solid-state lithium batteries: dispersion of garnet nanoparticles in insulating polyethylene oxide, Nano Energy 28 (2016) 447–454.
- [114] J. Zheng, M. Tang, Y.-Y. Hu, Lithium ion pathway within Li<sub>7</sub>La<sub>3</sub>Zr<sub>2</sub>O<sub>12</sub>-polyethylene oxide composite electrolytes, Angew. Chem. 128 (2016) 12726–12730
- [115] Y.W. Chen-Yang, H.C. Chen, F.J. Lin, C.C. Chen, Polyacrylonitrile electrolytes: 1. A novel high-conductivity composite polymer electrolyte based on PAN, LiClO<sub>4</sub> and  $\alpha$ -Al<sub>2</sub>O<sub>3</sub>, Solid State Ionics 150 (2002) 327–335.
- [116] C.R. Yang, J.T. Perng, Y.Y. Wang, C.C. Wan, Conductive behaviour of lithium ions in polyacrylonitrile, J. Power Sources 62 (1996) 89–93.
- [117] B. Huang, Z. Wang, G. Li, H. Huang, R. Xue, L. Chen, F. Wang, Lithium ion conduction in polymer electrolytes based on PAN, Solid State Ionics 85 (1996) 70, 84
- [118] B. Huang, Z. Wang, L. Chen, R. Xue, F. Wang, The mechanism of lithium ion transport in polyacrylonitrile-based polymer electrolytes, Solid State Ionics 91 (1996) 279–284.